

Limited predictability of amino acid substitutions in seasonal influenza viruses

Pierre Barrat-Charlaix,^{1,2} John Huddleston,³ Trevor Bedford,⁴ and Richard A. Neher^{1,2,*}

¹*Biozentrum, Universität Basel, Switzerland*

²*Swiss Institute of Bioinformatics, Basel, Switzerland*

³*Molecular Cell Biology, University of Washington, Seattle, WA, USA*

⁴*Vaccine and Infectious Disease Division, Fred Hutchinson Cancer Research Center, Seattle, WA, USA*

(Dated: July 31, 2020)

Seasonal influenza viruses repeatedly infect humans in part because they rapidly change their antigenic properties and evade host immune responses, necessitating frequent updates of the vaccine composition. Accurate predictions of strains circulating in the future could therefore improve the vaccine match. Here, we studied the predictability of frequency dynamics and fixation of amino acid substitutions. Current frequency was the strongest predictor of eventual fixation, as expected in neutral evolution. Other properties, such as occurrence in previously characterized epitopes or high *Local Branching Index* (LBI) had little predictive power. Parallel evolution was found to be moderately predictive of fixation. While the LBI had little power to predict frequency dynamics, it was still successful at picking strains representative of future populations. The latter is due to a tendency of the LBI to be high for consensus-like sequences that are closer to the future than the average sequence. Simulations of models of adapting populations, in contrast, show clear signals of predictability. This indicates that the evolution of influenza HA and NA, while driven by strong selection pressure to change, is poorly described by common models of directional selection such as travelling fitness waves.

INTRODUCTION

Seasonal influenza A viruses (IAV) infect about 10% of the global population every year, resulting in hundreds of thousands of deaths [1, 2]. Vaccination is the primary measure to reduce influenza morbidity. However, the surface proteins hemagglutinin (HA) and neuraminidase (NA) continuously accumulate mutations at a high rate, leading to frequent antigenic changes [2–5]. While a vaccine targeting a particular strain may be efficient for some time, antigenic drift will sooner or later render it obsolete. The World Health Organization (WHO) regularly updates influenza vaccine recommendations to best match the circulating strains. Since developing, manufacturing, and distributing the vaccine takes many months, forecasting the evolution of influenza is of essential interest to public health [6, 7].

The number of available high quality HA and NA sequences has increased rapidly over the last 20 years [8, 9] and virus evolution and dynamics can now be tracked at high temporal and spatial resolution [10]. This wealth of data has given rise to an active field of predicting influenza virus evolution [6, 7]. These models predict the future population of influenza viruses by estimating strain fitness or proxies of fitness. Luksza and Lässig [11], for example, train a fitness model to capture antigenic drift and protein stability on patterns of epitope and non-epitope mutations. Other approaches by Steinbrück et al. [12], Neher et al. [13] predict fitness by using hemagglutination inhibition (HI) data to determine possible

antigenic drift of clades in the genealogy of the HA protein. Finally, Neher et al. [14] use branching patterns of HA phylogenies as a proxy for fitness. These branching patterns are summarized by the Local Branching Index (LBI), which was shown to be a proxy of relative fitness in mathematical models of rapidly adapting populations [14].

The underlying assumption of all these methods is that (i) differences in growth rate between strains can be estimated from sequence or antigenic data and (ii) that these growth rate differences persist for long enough to be predictive of future success. Specific positions in surface proteins are of particular interest in this context. The surface proteins are under a strong positive selection and change their amino acid sequence much more rapidly than other IAV proteins or than expected under neutral evolution [4, 15]. Epitope positions, i.e., positions targeted by human antibodies, are expected to change particularly often since viruses with altered epitopes can evade existing immune responses [3, 5, 16]. It therefore seems plausible that mutations at these positions have a tendency to increase fitness and a higher probability of fixation [15]. But one has to be careful to account for the fact that these positions are often ascertained post-hoc [3] and human immune responses are diverse with substantial inter-individual variation [17].

In this work, we use HA and NA sequences of A/H3N2 and A/H1N1pdm influenza from year 2000 to 2019 to perform a retrospective analysis of frequency trajectories of amino acid mutations. We quantify how rapidly mutations at different frequencies are lost or fixed and how rapidly they spread through the population. We further investigate whether any properties or statistics are predictive of whether a particular mutation fixes or not. To our surprise, we find that the predictability of

* Correspondence to: Richard Neher, Biozentrum, Klingelbergstrasse 70, 4056, Basel, Switzerland. richard.neher@unibas.ch

these trajectories is very limited: The probability that a mutation fixes differs little from its current frequency, would be expected if fixation happened purely by chance. This observation holds for many different categories of mutations, including mutations at epitope positions. Weak predictability is not attributable solely to clonal interference and genetic linkage, as simulation of models including even strong interference retain clear signatures of predictability. Consistent with these observations, we show that a simple predictor uninformed by fitness, the consensus sequence, performs as well as the Local Branching Index (LBI), the growth measure based on the genealogy used in [14]. This suggests that although LBI has predictive power, the reason for its success may not be related to its approximating fitness of strains.

RESULTS

The main underlying question asked in this work is the following: given a mutation X in the genome of influenza that we observe at a frequency f in the population at a given date, what can we say about the future of X ? The trajectory of a mutation will depend on its own effect on fitness, the contribution of the genetic background on the same segment, and the effect of the remaining seven segments. Here, we investigate properties of broad categories of mutations effectively averaging over different genetic backgrounds to isolate the effects intrinsic to the mutation.

First, we ask whether we can quantitatively predict the frequency of X at future times $f(t)$. In other words, having observed a mutation at frequencies (f_1, f_2, \dots, f_n) at dates (t_1, t_2, \dots, t_n) , what can we say about its frequency at future dates $(t_{n+1}, t_{n+2}, \dots)$? A simpler, more qualitative question, is to ask whether X will fix in the population, will disappear, or whether the site will stay polymorphic.

We use amino-acid sequences of the HA and NA genes of A/H3N2 (since the year 2000) and A/H1N1pdm (since the year 2009) influenza available in GISAID [9] (see supplementary materials for an acknowledgment of all data contributors). This amounts to 44 976 HA and 36 300 NA sequences for A/H3N2 and 45 350 HA and 40 412 NA sequences for A/H1N1, with a minimum of 100 per year. These sequences are binned in non-overlapping intervals of one month. Each single-month time bin and the sequences that it contains represent a (noisy) snapshot of the influenza population at a given date. The number of sequences per time bin varies strongly both with year and according to the season, with earlier time bins containing around 10 sequences while more recent bins contain several hundreds (see figures S5 and S6 in SM for details).

The central quantities that we derived from this data are *frequency trajectories* of amino acids at each position in the sequences. If an amino acid X_i is found at position i at a frequency between 5% and 95% in the population of a given time bin t , then the population is considered

polymorphic at position i and at time t . This polymorphism is characterized by the frequency of X_i , $f_{X_i}(t)$, and also by frequencies of other amino acids at i . The series of values $f_{X_i}(t)$ for contiguous time bins constitutes the frequency trajectory of X_i . A trajectory is terminated if the corresponding frequency is measured above 95% (resp. below 5%) for two time bins in a row, in which case amino acid X_i is considered as *fixed* (resp. *absent*) in the population. Otherwise, the trajectory is considered *active*. Examples of trajectories can be seen in figure S7 of the Supplement.

In the rest of this work, we will focus on frequency trajectories that are starting at a zero (low) frequency, *i.e.* $f(t=0) = 0$. These represent new amino acid variants which were absent in the population at the time bin when the trajectory started and are currently rising in the population (see Methods). Such distinction in novel and ancestral variants is necessary to meaningfully interrogate predictability. Each rising trajectory of a new mutation implies the existence of another decreasing one at the same position, since frequencies of all amino acids at a given position must sum to one. If novel variants arise by selection, we expect to see a stronger signal of selection after conditioning on these novel variants. In classic models of population genetics, strongly advantageous variants undergo rapid selective *sweeps*, *i.e.*, the rapid rise and fixation. The sweep of a mutation can be due to its own fitness effect, to the genetic background or to the effect of the seven other segments. By considering the ensemble of novel variants that are rising in frequency, we effectively average over backgrounds, obtaining a set of mutations that we expect to be beneficial on average. If such sweeps are common in the evolution of HA and NA, the restriction to trajectories that start at low frequency should thus enrich for mutations that are positively selected and on their way to fixation.

Predicting future frequencies

Having observed the frequency trajectory $f(t)$ of a mutation until a given date t_0 , how much can we say about the future values of f after t_0 ? We consider the idealized case sketched in panel **A** of figure 1: given the trajectory of a *new* mutation, *i.e.* that started at a frequency of 0, and that we observe at frequency f_0 at time t_0 , what is the probability $P_{\Delta t}(f)$ of observing it at a value f at time $t_0 + \Delta t$?

To answer this question retrospectively, we use all frequency trajectories extracted from HA and NA sequences that satisfy these conditions for a given f_0 . The number of trajectories is limited and the frequency estimates themselves are based on a finite sample and are hence imprecise. Therefore, we consider trajectories in an interval $[f_0 - \delta f, f_0 + \delta f]$ with $\delta f = 0.05$.

For $f_0 = 0.3$, we found 120 such trajectories in the case of A/H3N2 influenza, represented on the panel **B** of figure 1, where time is shifted such that $t_0 = 0$. The

196 same analysis was performed for A/H1N1pdm, with the 89₂₅₄
197 found trajectories displayed in figure S9. Some trajectories
198 fall in the frequency bin around f_0 while decreasing, even₂₅₅
199 though they crossed that bin at an earlier time. This₂₅₆
200 is due to the fact that some trajectories “skipped” the₂₅₇
201 interval f_0 in question on their initial rise due to sparse₂₅₈
202 sampling. These trajectories are nevertheless rising in₂₅₉
203 the sense that they start at frequency 0 for $t \rightarrow -\infty$ ₂₆₀
204 Removing them does not change results significantly.₂₆₁

205 Since rapid sequence evolution of influenza HA and₂₆₂
206 NA mediates immune evasion, one could expect that₂₆₃
207 a significant fraction of new amino acid mutations on₂₆₄
208 rising trajectories in figure 1 are *adaptive*. We could thus₂₆₅
209 expect that most of these trajectories continue to rise after₂₆₆
210 reaching frequency f_0 , at least for some time. A fraction₂₆₇
211 of those would then sweep through the population and₂₆₈
212 fix.₂₆₉

213 To quantify the extent to which this preconception of₂₇₀
214 sweeping adaptive mutations is true, we estimated the₂₇₁
215 probability distribution $P_{\Delta t}(f|f_0)$ of finding a trajectory₂₇₂
216 at frequency f after a time Δt given that it was observed₂₇₃
217 at f_0 at time 0. The results for different Δt are shown in₂₇₄
218 figure 1C. Initially, *i.e.* at time $t_0 = 0$, this distribution is₂₇₅
219 by construction peaked around f_0 . If a large fraction of₂₇₆
220 the trajectories keep increasing after this time, we should₂₇₇
221 see the “mass” of $P_{\Delta t}(f|f_0)$ move to the right towards₂₇₈
222 higher frequencies as time progresses.₂₇₉

223 However, future distributions for $\Delta t > 0$ do not seem₂₈₀
224 to follow a pattern compatible with selective sweeps. The₂₈₁
225 thick black line in Figure 1B shows the average frequency₂₈₂
226 of all trajectories. This average makes a sharp turn at₂₈₃
227 $t = 0$ and is essentially flat for $t > 0$ in the case of₂₈₄
228 A/H3N2, and slightly increasing for A/H1N1pdm (see₂₈₅
229 supplement). Hence, the fact that this average rose for₂₈₆
230 $t < 0$ gives little information for $t > 0$, and is due to the₂₈₇
231 conditions by which these trajectories were selected. This₂₈₈
232 shows that sweep-like trajectories rising steadily from₂₈₉
233 frequency 0 to 1 are not common enough to dominate the₂₉₀
234 average trajectory.₂₉₁

235 Consistent with the average, the frequency distribution₂₉₂
236 of the selected trajectories broadens in time without a₂₉₃
237 significant shift of the mean as time passes. After 60 days₂₉₄
238 the distribution is rather symmetrical around the initial₂₉₅
239 $f_0 = 0.3$ value, suggesting that the knowledge that the₂₉₆
240 trajectories were rising is lost after two months. On a₂₉₇
241 timescale of 60 to 120 days, the only possible prediction₂₉₈
242 is that trajectories are likely to be found in a broad₂₉₉
243 interval around the initial frequency f_0 . After one year₃₀₀
244 the distribution becomes almost flat (excluding mutations₃₀₁
245 that have disappeared or fixed), and the initial peak at f_0 ₃₀₂
246 is not visible anymore. The only information remaining₃₀₃
247 from the initial frequency is the fraction that fixed or was₃₀₄
248 lost (see below). This behavior is expected in neutral₃₀₅
249 models of evolution [18] but incompatible with a dynamic₃₀₆
250 dominated by sweeps taking over the population.₃₀₇

251 While this observation does not rule out that signa-₃₀₈
252 tures exist that predict future frequency dynamics, past₃₀₉
253 dynamics alone is weakly informative.₃₁₀

Prediction of fixation or loss

Instead of predicting future frequency, let’s consider the long-term goal of predicting the probability that a mutation fixes in the population. We first estimate the fraction of frequency trajectories that either fix in the population or are lost, as well as the time it takes for one or the other to happen. Panels **A** and **B** of figure 2 shows the fraction of frequency trajectories in HA and NA that either have fixed, were lost or remained active as a function of the time elapsed since they were first seen above 25% frequency. Most mutations are either lost or become fixed after 2-3 years, with very few trajectories remaining active after 5 years. This time scale of 2-3 years is consistent with the typical coalescence time observed in phylogenetic trees of A/H3N2 influenza [10, 19]. We also note that the fraction of lost trajectories increases sharply at small times with 40% of mutations observed above 25% frequency being lost within one year for A/H3N2, while it takes longer to fix a mutation in the whole population.

We then examined the probability of mutations to fix in the population as a function of the frequency at which they are seen. For different values of frequency f , we consider all trajectories that started at a null frequency and are seen in the interval $[f - 7.5\%, f + 7.5\%]$ at any given time. The probability of a mutation fixing given that it is seen at frequency f , $P_{fix}(f)$, is then estimated by the fraction of those trajectories which terminate at a frequency larger than 95%, *i.e.* our fixation threshold. Panels **C** and **D** of figure 2 show $P_{fix}(f)$ as a function of f for NA and HA. For both proteins, the probability of fixation of a new mutation at frequency f is close to f itself, that is $P_{fix}(f) \simeq f$. This result is exactly what is expected in a population evolving in the *absence* of selection. A mutation or trait appearing at frequency f is shared by $f \cdot N$ individuals, and the probability for one of them to become the ancestor of all the future population is $f \cdot N/N = f$. Thus, the probability of this mutation or trait to fix in the population is equal to its current frequency, a case which we will refer to as the neutral expectation. Panel **C** of figure 2 indicates that mutations in the surface proteins of A/H3N2 influenza are in good agreement with the neutral expectation, while those in A/H1N1pdm show only small deviations from it. In both cases, the probability of fixation seems to be mainly dictated by the current frequency f at which the mutation is observed.

This dynamics is in apparent contradiction with evidence that influenza surface proteins are under strong selective pressure to evade human immune responses [4]. If strong selection was present, we would expect rising amino acid mutations to fix at a distinctively higher frequency than the one at which they are measured. In an extreme case where most trajectories would be clean sweeps, $P_{fix}(f)$ should be close to 1 for all but very small values of f .

Next, we searched for features of mutations that allow prediction of fixation beyond frequency by dividing

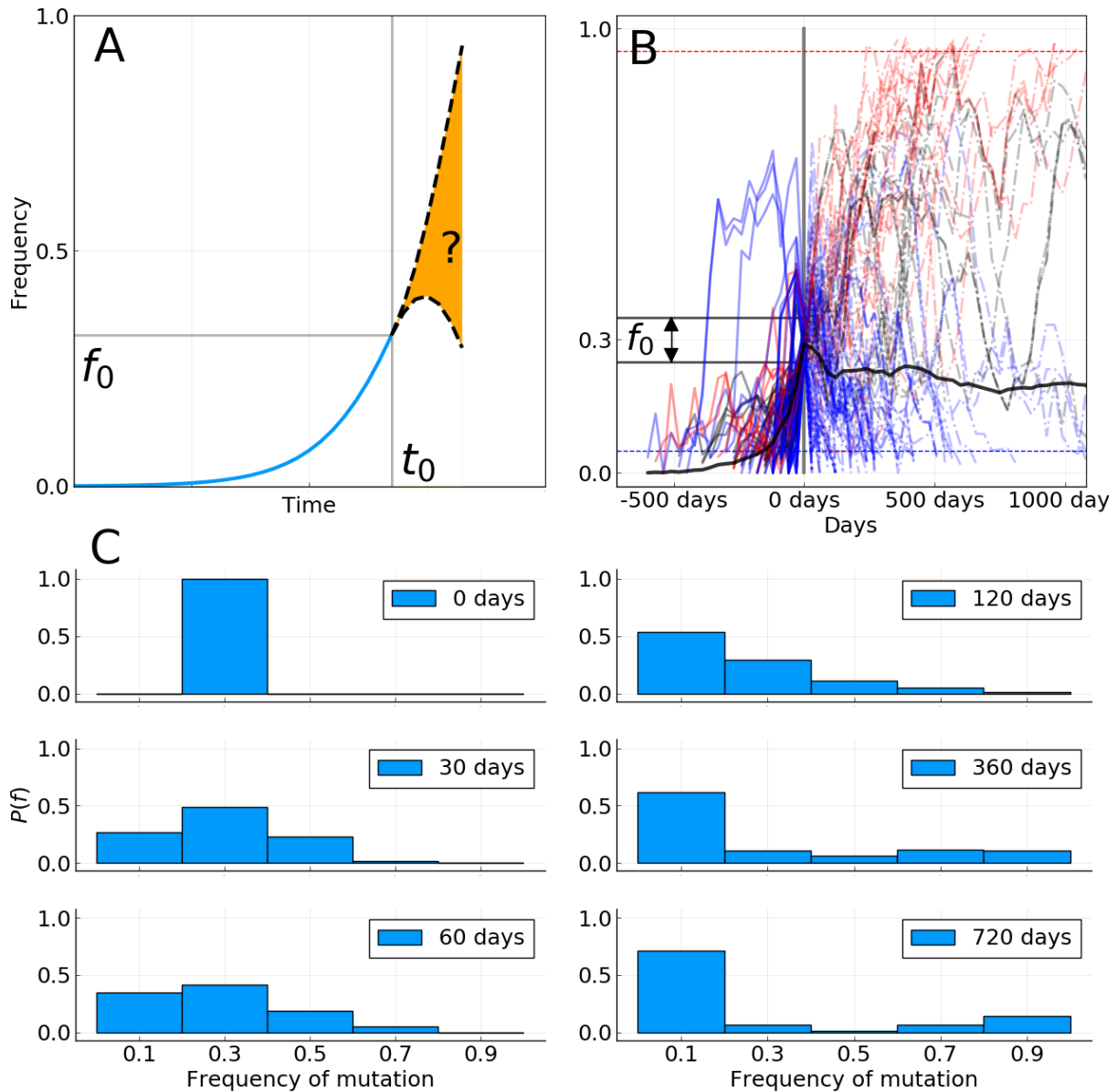


FIG. 1. **A:** Sketch of the idea behind the short term prediction of frequency trajectories. Given a mutation that we have seen increasing in frequency and that we “catch” at frequency f_0 at time t_0 , what can we say about the distribution of future frequencies $P_{\Delta t}(f|f_0)$? **B:** All frequency trajectories of amino acid mutations in the A/H3N2 HA and NA genes that were absent in the past, are seen around $f_0 = 30\%$ frequency at time $t_0 = 0$, and are based on more than 10 sequences at each time point. Red curves represent mutations that will ultimately fix, blue the ones that will be lost, and black the ones for which we do not know the final status. Dashed horizontal lines (blue and red) represent loss and fixation thresholds. The thick black line is the average of all trajectories, counting those that fix (resp. disappear) as being at frequency 1 (resp. 0). Figure S8 shows equivalent figures for other values of f_0 . **C:** Distribution of future frequencies $P_{\Delta t}(f|f_0)$ for the trajectories shown in panel **B** and for specific values of Δt .

311 frequencies into categories that deviate from the diag-318
 312 onal in panels **C** and **D** of figure 2. We first turn to 319
 313 the *Local Branching Index* (LBI), a quantity calculated 320
 314 for each node in a phylogenetic tree that indicates how 321
 315 dense the branching of the tree is around that node. LBI 322
 316 has previously been successfully used as a predictor of 323
 317 the future population of influenza [14], and was shown 324

to be a proxy for fitness of leaves or ancestral nodes in
 mathematical models of evolution. Here, we define the
 LBI of a mutation at date t as the average LBI of strains
 that carry this mutation and that were sampled in the
 time bin corresponding to t . Panel A of figure 3 shows
 fixation probability for HA mutations with LBI in the
 top or bottom half of the distribution. Both groups have

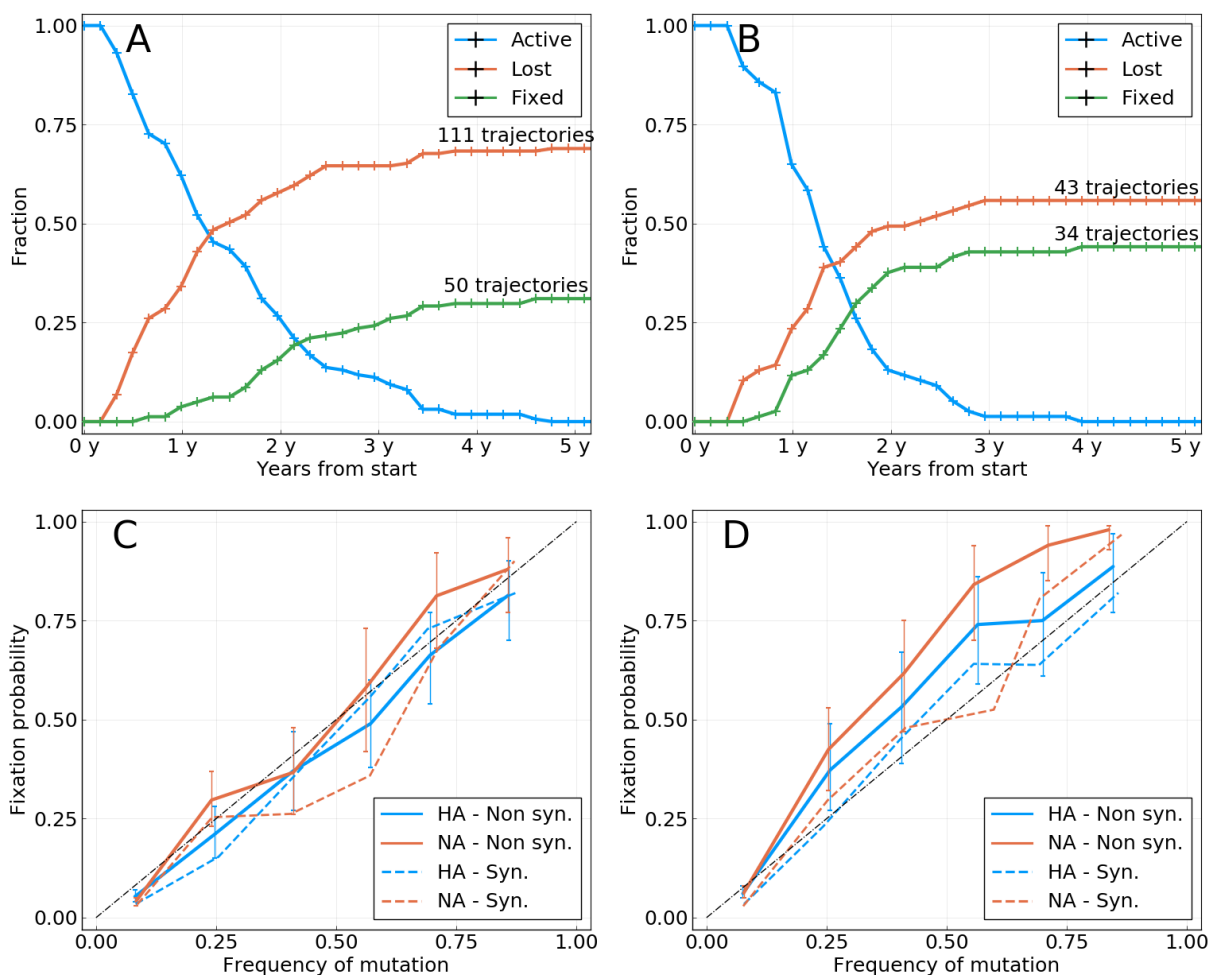


FIG. 2. **A:** Activity of all rising frequency trajectories seen above 25% frequency for A/H3N2 HA and NA. **B:** Same as **A** for A/H1N1. **C:** Probability of fixation of a mutation (amino acid or synonymous) $P_{fix}(f)$ as a function of the frequency f at which it is measured, for A/H3N2 HA and NA. Only new mutations are considered, *i.e.* mutations that were absent in the past. The diagonal dashed line is the expectation from a neutrally evolving population. Colored dashed lines represent synonymous mutations. Colored solid lines represent amino acid mutations. Error bars represent a 95% confidence interval. **D:** Same as **C** for A/H1N1.

325 identical probability of fixation, suggesting that LBI carries 342
 326 very little information on the probability of fixation 343
 327 of a mutation. 344

328 Next, we focused on previously reported antigenic sites 345
 329 in the A/H3N2 HA protein, referred to as *epitope* posi-346
 330 tions. Mutations at these position might mediate immune 347
 331 escape and are therefore likely under strong selection 348
 332 and show sweep-like behavior. We used four lists of rele-349
 333 vant epitope positions from different sources comprising 350
 334 from 7 to 129 positions in the sequence of the HA1 pro-351
 335 tein [3, 5, 11, 16]. Panel Fig. 3B shows fixation probability 352
 336 as a function of frequency for the four lists of epitopes 353
 337 Only mutations at the 7 epitope sites reported in [5] have 354
 338 higher chances of fixation than expected by chance. No 355
 339 clear difference is found for the lists by Luksza and Lässig 356
 340 [11], Wolf et al. [16], while positions from Shih et al. [3] 357
 341 show lower chances of fixation. One should also note that 358

many of these positions were determined post-hoc and might be enriched for positions that experienced rapid substitutions before the publication of the respective studies.

Two ways of categorising mutations, however, suggest some power to predict fixation. In panel Fig. 3C, we split trajectories into those occurring at binary positions where only two amino acid variants co-circulate and non-binary positions with more than two variants. Novel variants at non-binary positions, *i.e.* ones for which competition between three amino acids or more has occurred at least once, have a higher chance of fixation. In panel D, we separated mutations that appear more than once or only once in the reconstructed tree (see methods), and found that the former fix more often. Panels C and D show that it is possible to gain some information on the chance of fixation of a particular mutation, as was done in panel

359 **B.** However, the predictive power remains small, with⁴¹⁴
360 the “top” curves in panels **C&D** being very close to the⁴¹⁵
361 diagonal.⁴¹⁶

362 We conduct the same analysis on A/H1N1pdm⁴¹⁷
363 influenza, with results shown in figure S11. Results are⁴¹⁸
364 qualitatively similar to those obtained for A/H3N2, with⁴¹⁹
365 LBI giving little information and mutations at non-binary⁴²⁰
366 positions having a higher chance of fixation. Panel⁴²¹
367 **D** differs between figures 3 and S11, with convergent⁴²²
368 evolution giving less information on fixation in the latter⁴²³
369 case. However, this could be due to the shorter time⁴²⁴
370 period over which A/H1N1pdm evolved, resulting in a⁴²⁵
371 shorter tree and less possibilities of convergent evolution.⁴²⁶
372 Indeed, error bars for mutations appearing multiple times⁴²⁷
373 in **D** of figure S11 are relatively large, indicating a lower⁴²⁸
374 amount of trajectories.⁴²⁹
375⁴³⁰

376 Since influenza is seasonal in temperate regions, geo-⁴³¹
377 graphic spread and persistence might be predictive of the⁴³²
378 success of mutations. We quantify geographic spread of⁴³³
379 a mutation by the entropy of its frequency distribution⁴³⁴
380 across regions (see methods) and its persistence by the⁴³⁵
381 age of the trajectory by the time it reaches frequency f ⁴³⁶
382 Figures S12 and S13 show the fixation probabilities as⁴³⁷
383 a function of observed frequency for mutations classified⁴³⁸
384 according to these scores. The two scores also allow a⁴³⁹
385 quantitatively moderate distinction between mutations:⁴⁴⁰
386 for a given frequency f , mutations found in many regions⁴⁴¹
387 or those that are older (in the sense that they have taken⁴⁴²
388 more time to reach frequency f) tend to fix more often⁴⁴³
389 than geographically localized mutations or more recent⁴⁴⁴
390 ones, but the effect is small. These two scores are in⁴⁴⁵
391 fact correlated, with older trajectories representing mu-⁴⁴⁶
392 tations that are more geographically spread, as can be⁴⁴⁷
393 seen in figure S14 of SM. However, it is important to note⁴⁴⁸
394 that sampling biases and heterogeneity across time and⁴⁴⁹
395 space (see supplementary figures S5 and S6) make answer-⁴⁵⁰
396 ing such specific hypothesis challenging. Frequency of⁴⁵¹
397 mutations might thus be amplified through different sam-⁴⁵²
398 pling biases, making the connection between geographic⁴⁵³
399 spread, seasonality and mutation frequency non-trivial to⁴⁵⁴
400 measure.⁴⁵⁵
456
457
458
459

401 Simulations of models of adaptation

402 The results shown in figures 2 and 3 are difficult to⁴⁶⁰
403 reconcile with the idea that seasonal influenza virus evo-⁴⁶¹
404 lution is driven by rapid directed positive selection. One⁴⁶²
405 possible explanation for the weakly predictable behaviour⁴⁶³
406 of mutations (beyond their current frequency) might be⁴⁶⁴
407 tight genetic linkage inside each segment and strong com-⁴⁶⁵
408 petition between different adaptive mutations [15, 20].⁴⁶⁶
409 We design a simple model of population evolution based⁴⁶⁷
410 on the `ffpopsim` simulation software to test this hypoth-⁴⁶⁸
411 esis [21]. The model represents a population of binary⁴⁶⁹
412 genomes of length $L = 200$ evolving in a fitness landscape⁴⁷⁰
413 that changes through time.⁴⁷¹

First, we use an additive fitness function, with sequence
($x_1 \dots x_L$) having a fitness $\sum_i h_i x_i$. This implies that for
a given genome position i , the trait $x_i = 1$ is favored if
 $h_i > 0$ whereas $x_i = -1$ is favored if $h_i < 0$. All h_i 's
have the same magnitude, and only their signs matter.
Every Δt generations, we randomly choose a position i
and flip the sign of h_i , effectively changing the fitness
landscape. Individuals in the population now have the
opportunity to make an adaptive mutation at site i giving
them a fitness advantage $2|h|$. A “flip” at position i of the
fitness landscape will decrease fitness of all individuals
that carried the adapted variant at position i and increases
the fitness of those that happened to carry a deleterious
variant.

To increase competition between genomes, we designed
a second model that includes epistasis. Once again, the
baseline fitness of a genome is an additive function, this
time with values of h_i that do not change through time.
In addition, we added a component that mimics immune
selection. Every Δt generation, we now introduce “an-
tibodies” that target a specific sub-sequence of length
 $l = 5$, noted $(x_{i_1}^{ab}, \dots, x_{i_l}^{ab})$. The positions $(i_1 \dots i_l)$
are chosen at random, while the targeted sub-sequence is the
dominant state at each position. Genomes that include
the *exact* sub-sequence targeted by the antibody suffer a
strong fitness penalty. However, a single mutation away
from that sub-sequence removes this penalty completely,
resulting in a fitness landscape with very strong epista-
sis. This has the effect of triggering a strong competition
between adaptive mutations: for a given antibody, $l = 5$
possible mutations are now adaptive, but combinations
of these mutations do not bring any fitness advantage.

Having simulated populations in these two fitness land-
scapes, we perform the same analysis of frequency trajec-
tories as for the real influenza data. Figure S16 of the SM
shows the $P_{fix}(f)$ as a function of f for the two models
and for different values of the inverse rate of change Δt
of the fitness landscape. For all models, this curve devi-
ates significantly from the diagonal. This is most evident
for the case of a simple additive fitness landscape that
changes rarely $\Delta t = 1000$: rising mutations almost always
fix in the population, with $P_{fix}(f) \simeq 1$ for any f larger
than a few percent. This is corroborated by visual inspec-
tion of the trajectories, which shows that evolution in this
regime is driven by regular selective sweeps that take a
typical time of ~ 400 generations. In other regimes, with
smaller Δt or with strong epistatic competition, $P_{fix}(f)$
is reduced and closer to the diagonal. However, it takes
an extremely fast changing fitness landscape to push P_{fix}
close to the diagonal: with $\Delta t = 10$, that is about 40
changes to the fitness landscape in the time it would take
a selective sweep to go from 0% to fixation, $P_{fix}(f)$ differs
from f in a way that is comparable to what is observed
in A/H1N1pdm influenza.

These models are not meant to be accurate models of in-
fluenza viruses evolution. But figure S16 does show is that
the patterns observed in influenza virus evolution are only
reproduced by models of adapting populations when push-

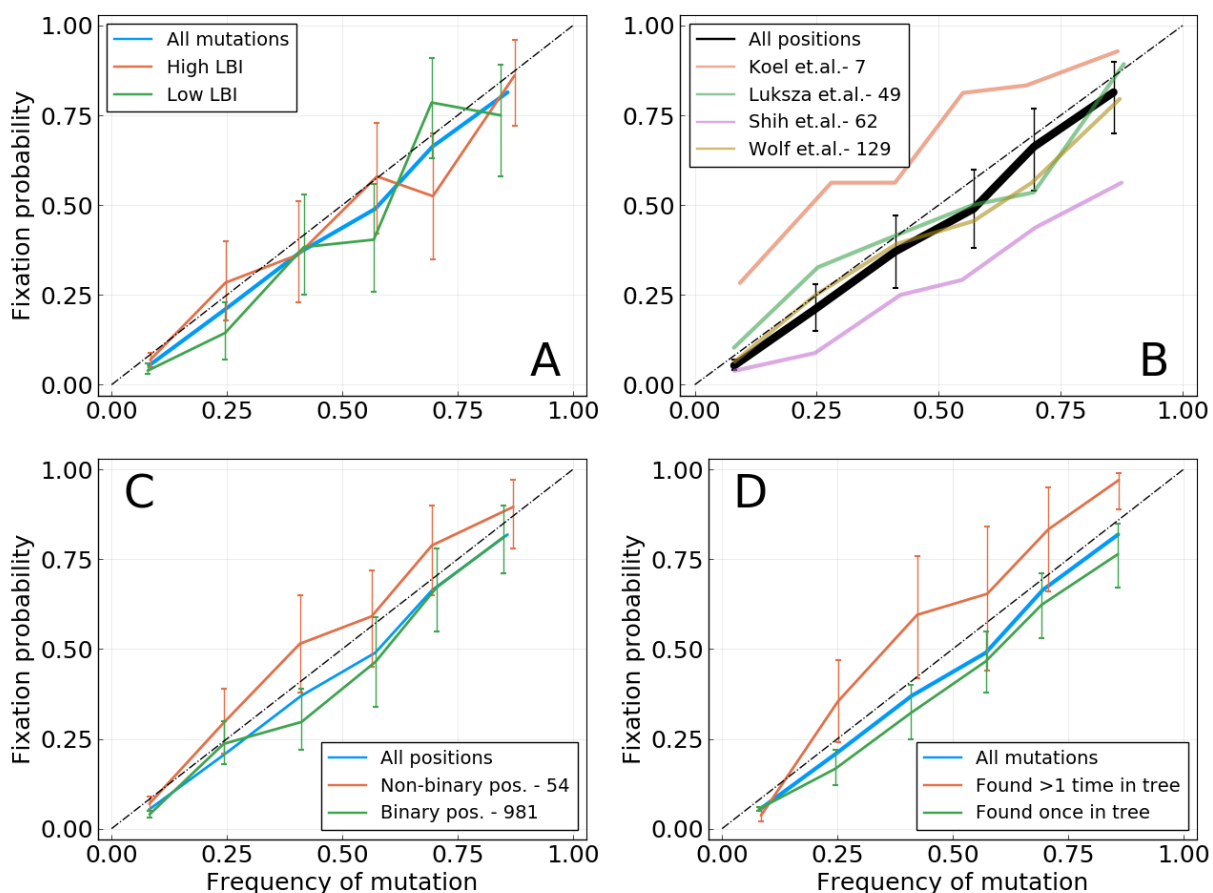


FIG. 3. Fixation probability $P_{fix}(f)$ as a function of frequency, for A/H3N2 influenza. Figure S11 shows the same analysis for A/H1N1. **A:** HA mutations with higher or lower LBI values, based on their position with respect to the median LBI value. **B:** Different lists of epitope positions in the HA protein. The authors and the number of positions is indicated in the legend. **C:** HA and NA mutations for binary positions, *i.e.* positions for which we never see more than two amino acids in the same time bin. **D:** HA and NA mutations that appear once or more than once in the tree for a given time bin.

472 ing clonal competition to extreme values. We conclude⁴⁹⁰
 473 that the pattern in figure 2 may not be a straightforward⁴⁹¹
 474 manifestation of genetic linkage and clonal interference,⁴⁹²
 475 but that some more intricate interplay of epidemiology,⁴⁹³
 476 seasonality, human immunity and chance gives rise to⁴⁹⁴
 477 the weakly predictable yet strongly selected evolutionary⁴⁹⁵
 478 dynamics of IAVs.

479 Why do predictions work?

480 The statistics of frequency trajectories seem to be in⁵⁰¹
 481 conflict with the notion that influenza evolution is pre-⁵⁰²
 482 dictable. Likewise, the LBI, a quantity that correlates⁵⁰³
 483 with fitness in mathematical models and is used to predict⁵⁰⁴
 484 future influenza populations [14], does not seem to contain⁵⁰⁵
 485 any information on whether a specific mutation is going⁵⁰⁶
 486 to fix or not, see figure 3. To resolve this conundrum, we⁵⁰⁷
 487 first note that the criterion by which predictive power for⁵⁰⁸
 488 influenza was measured in [14] was the distance between⁵⁰⁹
 489 the strain with the highest LBI and the future popula-⁵¹⁰

tion, not the ability of the LBI to predict dynamics. The
 distance was compared to the average distance between
 the present and future population, as well as the post-hoc
 optimal representative and the future.

To quantify the ability of the LBI and other measures
 to pick good representatives of the future, we construct
 a large tree of HA sequences with 100 sequences in non-
 overlapping time bins of 4 months from year 2003 to 2019
 (a total of 4402 as some 4 month intervals contain less
 than 100 sequences). Each time bin is considered as a
 snapshot of the A/H3N2 influenza population and we will
 refer to sequences in time bin t as the population of the
present. From this present population, we predict *future*
 populations in time bin $t + \Delta t$, using only sequences in
 time bin t and before.

To assess the ability of the LBI to pick a close represen-
 tative of the future, we compute the LBI of each node of
 one time bin in the tree using only the leaves that belong
 to that time bin. The top panel in figure 4 shows the
 hamming distance of the strain with the highest LBI to
 future populations at different Δt along with the same

511 distance for a randomly chosen strain. The figure shows⁵⁶⁶
512 the distance averaged over all possible values of t for Δt ⁵⁶⁷
513 between 0 and 32 months, giving us an average efficiency⁵⁶⁸
514 of a predictor over 16 years of influenza evolution.⁵⁶⁹

515 The strain with the highest LBI is consistently closer⁵⁷⁰
516 to the future than the average strain by about 1-2 amino⁵⁷¹
517 acids, while the overall distance increases linearly due to⁵⁷²
518 the continuous evolution of the population. We hence⁵⁷³
519 reproduce previous results showing that the LBI picks⁵⁷⁴
520 closer than average representatives [14]. To investigate⁵⁷⁵
521 whether this apparent success is due to the ability of the⁵⁷⁶
522 LBI to predict fitness or not, we explored a different pre-⁵⁷⁷
523 dictor: the amino acid consensus sequence of the present⁵⁷⁸
524 population (see Methods for a definition of the consensus⁵⁷⁹
525 sequence). The choice is motivated by the fact that it⁵⁸⁰
526 can be shown to be the best possible long term predictor⁵⁸¹
527 for a neutrally evolving population in terms of Hamming⁵⁸²
528 distance (see SM section 1). Figure 4 shows that the con-⁵⁸³
529 sensus sequence is in fact a equally good or even slightly⁵⁸⁴
530 better representative of the future than the sequence with⁵⁸⁵
531 highest LBI (note that the consensus sequence does *not*⁵⁸⁶
532 necessarily exist in the population).⁵⁸⁷

533 This near equivalence of the consensus and the strain⁵⁸⁸
534 with highest LBI can be explained as follows: The LBI⁵⁸⁹
535 tends to be high for nodes in a tree that are close to⁵⁹⁰
536 the root of a dense and large clade. A typical sample⁵⁹¹
537 of influenza HA sequences fall into a small number of⁵⁹²
538 recognizable clades, and the strains with maximal LBI⁵⁹³
539 will often be close to the root of the largest of those clades.⁵⁹⁴
540 This root of the largest clade will often be close to the⁵⁹⁵
541 consensus of the whole population, explaining the similar⁵⁹⁶
542 distance patterns. To test that hypothesis, we measure the⁵⁹⁷
543 hamming distance from the sequence of the top LBI strain⁵⁹⁸
544 to the consensus sequence for populations of all time bins.⁵⁹⁹
545 Panel **B** of figure 4 shows these distances, scaled with⁶⁰⁰
546 respect to an average strain (details in caption). It clearly⁶⁰¹
547 shows that the top-LBI strain and the consensus sequence⁶⁰²
548 are indeed quite similar: out of 48 time bins, only once⁶⁰³
549 is the sequence of the top-LBI strain farther away from⁶⁰⁴
550 the consensus than the average sequence is. Moreover,⁶⁰⁵
551 the sequence of the top-LBI strain *exactly* matches the⁶⁰⁶
552 consensus in 19 cases.⁶⁰⁷

553 DISCUSSION

554 Predicting the trajectory of a mutation requires (i)⁶¹²
555 significant fitness difference between genomes carrying⁶¹³
556 different variants at the site and (ii) a selection pressure⁶¹⁴
557 that changes slowly over time. Under such conditions, it is⁶¹⁵
558 expected that frequency trajectories will show a persistent⁶¹⁶
559 behavior which would make them predictable for some⁶¹⁷
560 time. However, we could find only limited evidence for⁶¹⁸
561 such persistent behavior in the past 19 years of IAV⁶¹⁹
562 evolution. This lead us to conclude that (i) influenza⁶²⁰
563 virus evolution is qualitatively different from models of⁶²¹
564 rapidly adapting population (despite clear evidence for⁶²²
565 frequent positive selection), and (ii) previous methods to⁶²³

predict influenza evolution work primarily because they
pick strains that represent the future well, not because
they predict future dynamics.

The primary focus in this work was the investigation
of frequency trajectories of new amino acid mutations.
In the short term, we found that on average the direction of
trajectory does not persist for longer than a few months.
Indeed, the average trajectory in figure 1 takes a sharp
turn when going from $t < 0$ to $t > 0$, instead of showing
“inertia”. This suggests that selective sweeps are not
representative of typical trajectories.

On a longer timescale, we investigated the probability
that a novel mutation observed at frequency f fixes. In
neutral models of evolution this probability equals f , while
it should be higher or lower than f for mutations with
a beneficial or deleterious effect on fitness, respectively.
However, in the case of influenza, this probability differs
little from f , making current frequency the best predictor
for fixation. In figure 3, we split trajectories into groups
for which we expected P_{fix} to deviate from f . Many of
these splits, such as high/low LBI or epitope/non-epitope
positions, did not result in an increased predictability,
while others gave limited information on fixation. Despite
the lack of predictability of mutation frequency trajecto-
ries, influenza surface proteins show strong signatures of
selection [4, 15].

Methods for predicting the future evolution of influenza
either construct explicit fitness models [11, 22], use his-
torical patterns of evolution [11, 23], phenotypic assays
[13, 24], or dynamic or phylogenetic patterns [14, 25]. The
goal of these methods is to pick strains that are good
representatives of future populations and could serve as
vaccine candidates [6].

The low power to predict frequency dynamics or fixation
naturally triggers the question why the above methods
have been found to work. Picking representatives of the
future and predicting frequency dynamics are distinct
objectives and success at the former (as compared to ran-
dom picks) is not necessarily inconsistent with a lack of
predictable dynamics. In fact, [22] reports that the rate
at which the frequency of a strain changes is often a poor
predictor – consistent with our observations here. But
despite the fact that future frequencies are not predicted
by the LBI, the strain with the highest LBI in the popu-
lation is a better predictor of the future population than
a randomly picked one. While the LBI was shown to be a
correlate of relative fitness and be predictive of fixation in
mathematical models of evolution [14], it does not seem
to be predict influenza evolution because it measures fit-
ness from genealogical structure. Instead, we believe it
picks closer than average strains simply because it has the
tendency to be maximal at the base of large and dense
clades. These basal genotypes are closer to the future
populations than the current tips of the tree and hence
a better predictor on average. The consensus sequence
of all present strains performs slightly but consistently
better than picking the strain with the highest LBI. The
consensus sequence is the best possible predictor for a

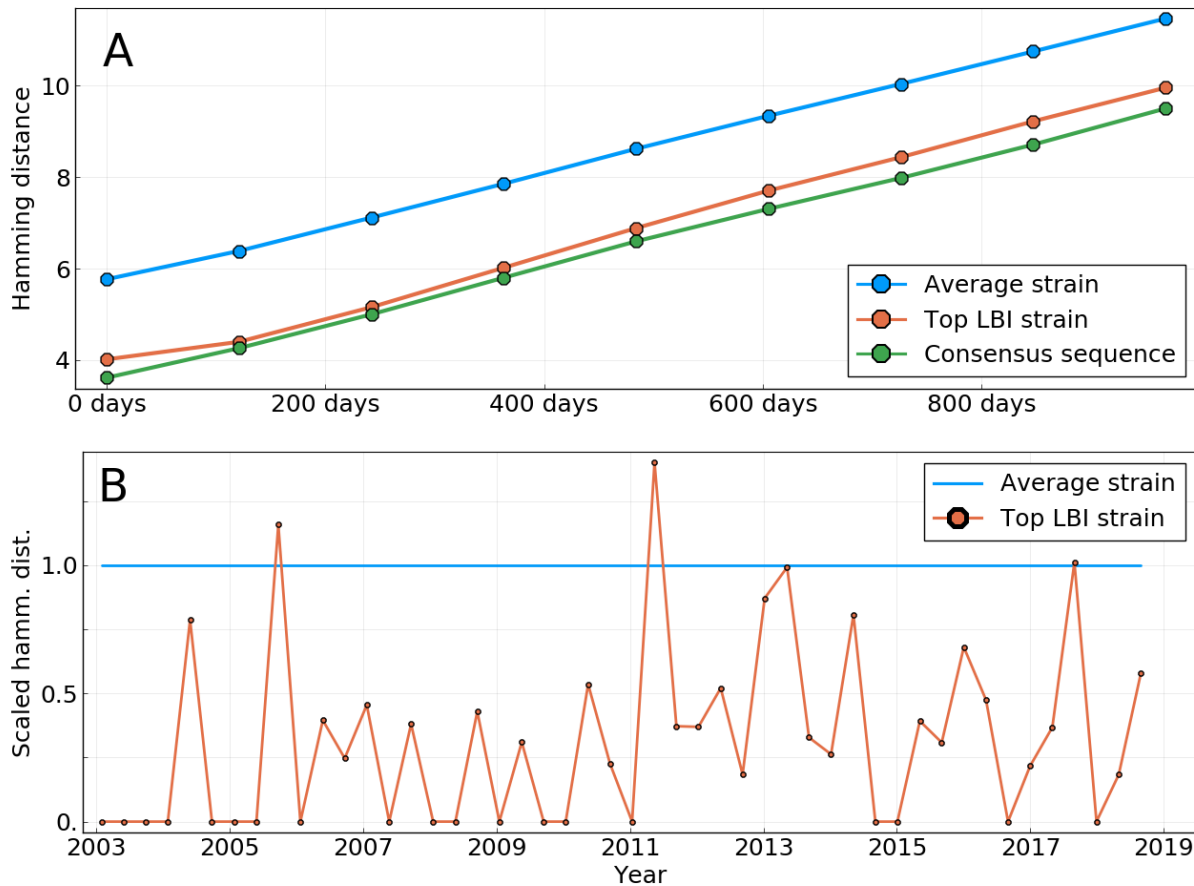


FIG. 4. **A**: Average Hamming distance of the sequences of different predictors to HA sequences of future influenza populations, themselves averaged over all “present” populations from year 2003 to 2019. Predictors are: a randomly picked sequence in the present population; the sequence of the strain with the highest LBI in the present population; the consensus sequence of the present population. **B**: Scaled Hamming distance between the sequence of the top LBI strain and the consensus sequence for populations at different dates. The scaling is such that for each date, the Hamming distance between a strain from the population and the consensus is on average 1. The strain with the highest LBI is almost always closer to the consensus sequence than the average strain.

624 neutrally evolving population, and does not attempt to 643
 625 model fitness in any way. 644

626 At the same time, influenza virus phylogenies show clear 645
 627 deviations from those expected from the neutral Kingman 646
 628 coalescent, similar to those expected under Bolthausen- 647
 629 Sznitman coalescent (BSC) processes that are generated 648
 630 by traveling wave models of rapid evolution [26, 27]. The 649
 631 correspondence between the BSC and traveling wave mod- 650
 632 els comes from transient exponential amplification of fit 651
 633 strains before these fitness differences are wiped out by 652
 634 further mutation. This exponential amplification gen- 653
 635 erates long-tailed effective offspring distributions which 654
 636 in turn can leads to genealogies described by the BSC 655
 637 [26, 28]. Many processes other than selection, includ- 656
 638 ing seasonality and spatio-temporal heterogeneity, can
 639 generate effective long tailed offspring distributions even
 640 in absence of bona-fide fitness differences, which might
 641 explain ladder-like non-Kingman phylogenetic trees.

642 A recent preprint proposed that influenza virus evo-

lution is primarily limited by an asynchrony between
 population level selection and generation of new variants
 within infected hosts [29]. Along these lines, it is possi-
 ble that the A/H3N2 population readily responds once
 population level selection is high enough by giving rise
 to essentially equivalent variants. Furthermore, selection
 might cause the rapid rise of a novel variant to macro-
 scopic frequencies (observable in a global sample) but
 its benefit rapidly “expires” because competing variants
 catch up and/or it mediates immune escape only to a
 small fraction of the population. These considerations
 might explain the disconnect between models of rapid
 adaptation and the frequency dynamics observed in in-
 fluenza virus populations.

METHODS

Data and code availability

The sequences used are obtained from the GISAID database [9]. Strain names and accession numbers are given as tables in two supplementary files. Outliers strains listed at <https://github.com/PierreBarrat/FluPredictibility/src/config> were removed. The code used to generate the figures presented here is available at <https://github.com/PierreBarrat/FluPredictibility>.

Frequency trajectories

For a set of sequences in a given time bin, we compute frequencies of amino acids at each position by simple counting. We make the choice of not applying any smoothing method in an attempt to be as close to the data and “model-less” as possible. This is especially important for the short term prediction of frequency trajectories, as estimations of the “persistence time” of a trajectory might be biased by a smoothing method.

We compute frequency trajectories based on the frequencies of amino acids. A trajectory begins at time t if an amino acid is seen under the lower frequency threshold of 5% (resp. above the higher threshold of 95%) for the two time bins preceding t , and above this lower threshold (resp. below the higher threshold) for time bin t . It ends in the reciprocal situation, that is when the frequency is measured below the lower threshold (resp. above the higher threshold) for two time bins in a row.

In order to avoid estimates of frequencies that are too noisy, we only keep trajectories that are based on a population of at least 10 sequences for *each* time bin. As said in the Results section, we also restrict the analysis to trajectories that begin at a 0 frequency, in part to avoid double counting. We find a total of 460 such trajectories. However, only 106 reach a frequency of 20%, on which figure 2 is based for instance.

Note that the fact that we use samples of relatively small sizes – at least for some time bins – leads to biases in the estimation of frequencies. We show in Supplementary Material that these biases are generally small and do not induce any qualitative changes to results presented here.

Local Branching Index

LBI was introduced in [14] as an approximation of fitness in populations evolving under persistent selective pressure that is fully based on a phylogenetic tree. It relies on the intuition that the tree below high-fitness individuals will show dense branching events, whereas absence of branching is a sign of low-fitness individuals. Quantitatively, the LBI $\lambda_i(\tau)$ of a node i is the integral

of all of the tree’s branch length around i , with an exponentially decreasing weight $e^{-t/\tau}$ with t being the branch length. When considering a time binned population, the LBI is computed once for each time bin by considering only the leaves of the tree that belong to the time bin. This means that only branches that ultimately lead to a leaf that belongs to the time bin are considered in the integration.

τ is the time scale for which the tree is informative of the fitness of a particular node. Here, we use a value of τ equal to a tenth of $T_C \simeq 6$ years, the coalescence time for influenza A/H3N2 strains, converted to units of tree branch length through the average nucleotide substitution rate ($\simeq 4 \cdot 10^{-3}$ substitutions per site per year for HA). We have observed that given our method to predict the future from present populations corresponding to time bins of 4 months, changing the value of τ has little effect on the pick of the top LBI strain. By retrospectively optimizing its value, it is possible to reduce the average distance to the population 2 years ahead by ~ 0.25 amino acids on average, making the LBI method almost as good as the consensus on figure 4.

Measuring the geographical spread of a mutation

For a mutation X we define its regional distribution using the numbers $n_r(X)$ that represent the number of sequences sampled in region r that carry X . Regional weights are then defined as

$$w_r(X) = \frac{n_r(X)}{\sum_r n_r(X)}.$$

We can then measure the geographical spread $G(X)$ of X by using the Shannon entropy of the probability distribution $w_r(X)$:

$$G(X) = \sum_r w_r(X) \log(w_r(X)).$$

$G(X)$ is a positive quantity that is larger when X is equally present in many regions, and equal to zero when X is concentrated in only one region.

Region used are the ones defined in the Nextstrain tool [30]. Those are North America, South America, Europe, China, Oceania, Southeast Asia, Japan & Korea, South Asia, West Asia, and Africa.

Assigning a fitness to trajectories

Consensus sequence

Given a set of N sequences ($\sigma^1, \dots, \sigma^N$) based on an alphabet \mathcal{A} (e.g. \mathcal{A} has 20 elements for amino acids, 4 for nucleotides), we can define a *profile* distribution $p_i(a)$

by the following expression:

$$p_i(a) = \sum_{n=1}^N \delta_{\sigma_i^n, a}$$

where i is a position in the sequence, σ_i^n the character appearing at position i in sequence σ^n , a a character of the alphabet and δ the Kronecker delta. The profile $p_i(a)$ simply represents the fraction of sequences which have character a at position i .

We then simply define the consensus sequence σ^{cons} such that

$$\sigma_i^{cons} = \operatorname{argmax}_a p_i(a).$$

738 In other words, the consensus sequence is the one that
739 has the dominant character of the initial set of sequences
740 at each position.

741 Earth Mover's Distance

In order to measure the distance of several predictor745
sequences to the future population, we rely on the *Earth*746
Mover's Distance (EMD), a metric commonly applied747
in machine learning to compare collections of pixels or748
words [31, 32]. Here, we apply it to compute the dis749
tance between the sequences of two populations, noted as750

$\mathcal{X} = \{(x^n, p^n)\}$ and $\mathcal{Y} = \{(y^m, q^m)\}$ with $n \in \{1 \dots N\}$
and $m \in \{1 \dots M\}$. In this notation, x^n and y^m are
sequences, and p^n and q^m are the frequencies at which
these sequences are found in their respective populations.
For convenience, we also define $d_{nm} = H(x^n, y^m)$ as the
Hamming distance between pairs of sequences in the two
populations.

We now introduce the following functional

$$F(\mathbf{w}) = \sum_{n,m} d_{nm} w_{nm},$$

with $\mathbf{w} = \{w_{nm}\}$ being a matrix of positive weights. The
EMD between the two populations \mathcal{X} and \mathcal{Y} is now defined
as the minimum value of function F under the conditions

$$\sum_{n=1}^N w_{nm} = q^m, \quad \sum_{m=1}^M w_{nm} = p^n, \quad \text{and} \quad w_{nm} \geq 0$$

742 Intuitively, the weight w_{nm} tells us how much of sequence
743 x^n is “moved” to sequence y^m . The functional F sums
744 all of these moves and attributes them a cost equal to
the Hamming distance d_{nm} . The conditions on weights
in \mathbf{w} ensure that all the weight p^n of x^n is “moved” to
elements in \mathcal{Y} and vice versa.

The minimization is easily performed by standard linear
optimization libraries. Here, we use the Julia library
JuMP [33].

-
- 751 [1] World Health Organization, 2018. URL [https://www.who.int/fr/news-room/fact-sheets/detail/](https://www.who.int/fr/news-room/fact-sheets/detail/influenza-(seasonal))
752 [influenza-\(seasonal\)](https://www.who.int/fr/news-room/fact-sheets/detail/influenza-(seasonal)).
753
754 [2] Velislava N. Petrova and Colin A. Russell. The evolution
755 of seasonal influenza viruses. *Nature Reviews Microbiology*,
756 16(1):47–60, October 2017. ISSN 1740-1526, 1740-1534
757 doi:10.1038/nrmicro.2017.118. URL [http://www.nature](http://www.nature.com/doifinder/10.1038/nrmicro.2017.118)
758 [com/doifinder/10.1038/nrmicro.2017.118](http://www.nature.com/doifinder/10.1038/nrmicro.2017.118).
759 [3] Arthur Chun-Chieh Shih, Tzu-Chang Hsiao, Mei-Shang
760 Ho, and Wen-Hsiung Li. Simultaneous amino acid sub-
761 stitutions at antigenic sites drive influenza a hemagglu-
762 tinin evolution. *Proceedings of the National Academy*
763 *of Sciences*, 104(15):6283–6288, 2007. ISSN 0027-8424
764 doi:10.1073/pnas.0701396104. URL [https://www.pnas](https://www.pnas.org/content/104/15/6283)
765 [org/content/104/15/6283](https://www.pnas.org/content/104/15/6283).
766 [4] Samir Bhatt, Edward C. Holmes, and Oliver G. Pybus
767 The Genomic Rate of Molecular Adaptation of the Human
768 Influenza A Virus. *Molecular Biology and Evolution*, 28
769 (9):2443–2451, September 2011. ISSN 0737-4038. doi:
770 10.1093/molbev/msr044. URL [https://academic.oup](https://academic.oup.com/mbe/article/28/9/2443/1007907)
771 [com/mbe/article/28/9/2443/1007907](https://academic.oup.com/mbe/article/28/9/2443/1007907).
772 [5] Björn F. Koel, David F. Burke, Theo M. Bestebroer,
773 Stefan van der Vliet, Gerben C. M. Zondag, Gaby Vervae-
774 t Eugene Skepner, Nicola S. Lewis, Monique I. J. Spronken,
775 Colin A. Russell, Mikhail Y. Eroshin, Aeron C. Hurt,
776 Ian G. Barr, Jan C. de Jong, Guus F. Rimmelzwaan,
777 Albert D. M. E. Osterhaus, Ron A. M. Fouchier, and
778 Derek J. Smith. Substitutions near the receptor binding
779 site determine major antigenic change during influenza
virus evolution. *Science*, 342(6161):976–979, 2013. ISSN
0036-8075. doi:10.1126/science.1244730. URL <https://science.sciencemag.org/content/342/6161/976>.
[6] Dylan H Morris, Katelyn M Gostic, Simone Pompei,
Trevor Bedford, Marta Luksza, Richard A Neher, Bryan T
Grenfell, Michael Lässig, and John W McCauley. Predic-
tive modeling of influenza shows the promise of applied
evolutionary biology. *Trends in microbiology*, 26(2):102–
118, 2018.
[7] Thorsten R. Kligen, Susanne Reimering, Carlos A.
Guzmán, and Alice C. McHardy. In Silico Vaccine
Strain Prediction for Human Influenza Viruses. *Trends*
in Microbiology, 26(2):119–131, February 2018. ISSN
0966-842X. doi:10.1016/j.tim.2017.09.001. URL
[http://www.sciencedirect.com/science/article/](http://www.sciencedirect.com/science/article/pii/S0966842X17302068)
[pii/S0966842X17302068](http://www.sciencedirect.com/science/article/pii/S0966842X17302068).
[8] Peter Bogner, Ilaria Capua, David J Lipman, and Nancy J
Cox. A global initiative on sharing avian flu data. *Nature*,
442(7106):981–981, 2006.
[9] Yuelong Shu and John McCauley. Gisaid: Global initia-
tive on sharing all influenza data—from vision to reality.
Eurosurveillance, 22(13), 2017.
[10] Andrew Rambaut, Oliver G. Pybus, Martha I. Nelson,
Cecile Viboud, Jeffery K. Taubenberger, and Edward C.
Holmes. The genomic and epidemiological dynamics of
human influenza A virus. *Nature*, 453(7195):615–619, May
2008. ISSN 1476-4687. doi:10.1038/nature06945. URL
<https://www.nature.com/articles/nature06945>.

- [11] Marta Luksza and Michael Lässig. A predictive fitness model for influenza. *Nature*, 507(7490):57–61, March 2014. ISSN 1476-4687. doi:10.1038/nature13087. URL <https://www.nature.com/articles/nature13087>. Number: 7490. Publisher: Nature Publishing Group.
- [12] L. Steinbrück, T. R. Klingen, and A. C. McHardy. Computational prediction of vaccine strains for human influenza A (h3n2) viruses. *Journal of Virology*, 88(20):12123–12132, 2014. ISSN 0022-538X. doi:10.1128/JVI.01861-14. URL <https://jvi.asm.org/content/88/20/12123>.
- [13] Richard A. Neher, Trevor Bedford, Rodney S. Daniels, Colin A. Russell, and Boris I. Shraiman. Prediction dynamics, and visualization of antigenic phenotypes of seasonal influenza viruses. *Proceedings of the National Academy of Sciences of the United States of America*, 113(12):E1701–1709, March 2016. ISSN 1091-6490 0027-8424. doi:10.1073/pnas.1525578113.
- [14] Richard A Neher, Colin A Russell, and Boris I Shraiman. Predicting evolution from the shape of genealogical trees. *eLife*, 3, November 2014. ISSN 2050-084X. doi:10.7554/eLife.03568. URL <https://www.ncbi.nlm.nih.gov/pmc/articles/PMC4227306/>.
- [15] Natalja Strelkova and Michael Lässig. Clonal interference in the Evolution of Influenza. *Genetics*, 192(2):671–682, October 2012. ISSN 0016-6731, 1943-2631. doi:10.1534/genetics.112.143396. URL <http://www.genetics.org/content/192/2/671>.
- [16] Yuri I Wolf, Cecile Viboud, Edward C Holmes, Eugene V Koonin, and David J Lipman. Long intervals of stasis punctuated by bursts of positive selection in the seasonal evolution of influenza A virus. *Biology Direct*, 1:34, October 2006. ISSN 1745-6150. doi:10.1186/1745-6150-1-34. URL <https://www.ncbi.nlm.nih.gov/pmc/articles/PMC1647279/>.
- [17] Juhye M Lee, Rachel Eguia, Seth J Zost, Saket Choudhary, Patrick C Wilson, Trevor Bedford, Terry Stevens Ayers, Michael Boeckh, Aeron C Hurt, Seema S Lakdawala, Scott E Hensley, and Jesse D Bloom. Mapping person-to-person variation in viral mutations that escape polyclonal serum targeting influenza hemagglutinin. *eLife*, 8:e49324, August 2019. ISSN 2050-084X. doi:10.7554/eLife.49324. URL <https://doi.org/10.7554/eLife.49324>. Publisher: eLife Sciences Publications, Ltd.
- [18] Motoo Kimura. Diffusion Models in Population Genetics. *Journal of Applied Probability*, 1(2):177–232, 1964. ISSN 0021-9002. doi:10.2307/3211856. URL <http://www.jstor.org/stable/3211856>.
- [19] Le Yan, Richard A Neher, and Boris I Shraiman. Phylogenetic theory of persistence, extinction and speciation of rapidly adapting pathogens. *eLife*, 8:e44205, September 2019. ISSN 2050-084X. doi:10.7554/eLife.44205. URL <https://doi.org/10.7554/eLife.44205>. Publisher: eLife Sciences Publications, Ltd.
- [20] R. A. Neher and B. I. Shraiman. Genetic draft and quasi-neutrality in large facultatively sexual populations. *Genetics*, 188(4):975–996, August 2011. ISSN 1943-2631 0016-6731. doi:10.1534/genetics.111.128876.
- [21] Fabio Zanini and Richard A. Neher. FFPopSim: an efficient forward simulation package for the evolution of large populations. *Bioinformatics*, 28(24):3332–3333, 10 2012. ISSN 1367-4803. doi:10.1093/bioinformatics/bts633. URL <https://doi.org/10.1093/bioinformatics/bts633>.
- [22] John Huddleston, John R. Barnes, Thomas Rowe, Rebecca Kondor, David E. Wentworth, Lynne Whittaker, Burcu Ermetal, Rodney S. Daniels, John W. McCauley, Seiichiro Fujisaki, Kazuya Nakamura, Noriko Kishida, Shinji Watanabe, Hideki Hasegawa, Ian Barr, Kanta Subbarao, Richard Neher, and Trevor Bedford. Integrating genotypes and phenotypes improves long-term forecasts of seasonal influenza A/H3N2 evolution. *bioRxiv*, page 2020.06.12.145151, June 2020. doi:10.1101/2020.06.12.145151. URL <https://www.biorxiv.org/content/10.1101/2020.06.12.145151v1>. Publisher: Cold Spring Harbor Laboratory Section: New Results.
- [23] R. M. Bush, C. A. Bender, K. Subbarao, N. J. Cox, and W. M. Fitch. Predicting the evolution of human influenza A. *Science (New York, N.Y.)*, 286(5446):1921–1925, December 1999. ISSN 0036-8075.
- [24] Lars Steinbrück and Alice Carolyn McHardy. Inference of Genotype–Phenotype Relationships in the Antigenic Evolution of Human Influenza A (H3N2) Viruses. *PLoS Computational Biology*, 8(4):e1002492, April 2012. ISSN 1553-7358. doi:10.1371/journal.pcbi.1002492. URL <http://journals.plos.org/ploscompbiol/article?id=10.1371/journal.pcbi.1002492>.
- [25] Thorsten R. Klingen, Susanne Reimering, Jens Loers, Kyra Mooren, Frank Klawonn, Thomas Krey, Gülsah Gabriel, and Alice C. McHardy. Sweep Dynamics (SD) plots: Computational identification of selective sweeps to monitor the adaptation of influenza A viruses. *Scientific Reports*, 8(1):373, January 2018. ISSN 2045-2322. doi:10.1038/s41598-017-18791-z. URL <https://www.nature.com/articles/s41598-017-18791-z>.
- [26] Richard A. Neher and Oskar Hallatschek. Genealogies of rapidly adapting populations. *Proceedings of the National Academy of Sciences of the United States of America*, 110(2):437–442, January 2013. ISSN 1091-6490 0027-8424. doi:10.1073/pnas.1213113110.
- [27] Michael M. Desai, Aleksandra M. Walczak, and Daniel S. Fisher. Genetic Diversity and the Structure of Genealogies in Rapidly Adapting Populations. *Genetics*, 193(2):565–585, February 2013. ISSN 0016-6731, 1943-2631. doi:10.1534/genetics.112.147157. URL <http://www.genetics.org/content/193/2/565>.
- [28] Jason Schweinsberg. Coalescent processes obtained from supercritical Galton–Watson processes. *Stochastic Processes and their Applications*, 106(1):107–139, July 2003. ISSN 0304-4149. doi:10.1016/S0304-4149(03)00028-0. URL <http://www.sciencedirect.com/science/article/pii/S0304414903000280>.
- [29] Dylan H. Morris, Velislava Petrova, Fernando W. Rossine, Edyth Parker, Bryan Grenfell, Richard Neher, Simon Levin, and Colin Russell. Asynchrony between virus diversity and antibody selection limits influenza virus evolution. preprint, Open Science Framework, April 2020. URL <https://osf.io/847p2>.
- [30] James Hadfield, Colin Megill, Sidney M Bell, John Huddleston, Barney Potter, Charlton Callender, Pavel Sagulenko, Trevor Bedford, and Richard A Neher. Nextstrain: real-time tracking of pathogen evolution. *Bioinformatics*, 34(23):4121–4123, 05 2018. ISSN 1367-4803. doi:10.1093/bioinformatics/bty407. URL <https://doi.org/10.1093/bioinformatics/bty407>.
- [31] Y. Rubner, C. Tomasi, and L. J. Guibas. A metric for distributions with applications to image databases. In *Sixth International Conference on Computer Vision (IEEE Cat. No.98CH36271)*, pages 59–66, Jan 1998. doi:

- 936 10.1109/ICCV.1998.710701. 944
- 937 [32] Matt J. Kusner, Yu Sun, Nicholas I. Kolkin, and Kil-945
 938 ian Q. Weinberger. From word embeddings to document946
 939 distances. In *Proceedings of the 32nd International Con-947*
 940 *ference on International Conference on Machine Learning948*
 941 *- Volume 37*, ICML'15, page 957–966. JMLR.org, 2015. 949
- 942 [33] Iain Dunning, Joey Huchette, and Miles Lubin. Jump: A950
 943 modeling language for mathematical optimization. *SIAM951*
952
- Review*, 59(2):295–320, 2017. doi:10.1137/15M1020575.
- [34] Julia Sigwart. Gene Genealogies, Variation and Evo-
 lution: A Primer in Coalescent Theory.—Jotun Hein,
 Mikkel H. Schierup, and Carsten Wiuf. 2004. Oxford Uni-
 versity Press, Oxford. xiii + 276 pp. ISBN 0-19-852996-1,
 £29.95 (paperback); ISBN 0-19-852995-3, £65.00 (hard-
 back). *Systematic Biology*, 54(6):986–987, 12 2005. ISSN
 1063-5157. doi:10.1080/10635150500354860. URL <https://doi.org/10.1080/10635150500354860>.

SUPPLEMENTARY MATERIAL

1. Consensus sequence as a predictor for neutrally evolving populations

955 We consider the case of a neutrally evolving and structure-less population, such as the one in the Wright-Fisher
 956 model of evolution [34]. At an initial time $t = 0$, the population consists of N individuals with genomes $(\sigma^1 \dots \sigma^N)$ of
 957 length L (not necessarily distinct).

958 We make two hypotheses about this population. We first suppose that *no* mutations occur during the evolution of this
 959 population. This may seem surprising and is of course not true in the case of influenza. This assumption is however in
 960 line with the fact that the object of this work is to predict the outcome of *already existing* mutations in the influenza
 961 population. The prediction of mutations that we have not yet seen is not in its scope. Thus, assuming that no new
 962 mutations take place can be seen as a simple way to model the fact that we have no information about such events.
 963 The second assumption is that the population evolves in a completely neutral way, meaning that the average number
 964 of descendants of each genome σ^n is the same. Let us now consider the population after it has evolved for a long time
 965 $t \gg T$ where T is the typical coalescence time (for the Wright-Fisher model, $T = 2N$). At this point, all individuals in
 966 the future population will descend from a unique individual n_0 in the $t = 0$ population. Our two hypotheses now allow
 967 us to make two statements. First, since no new mutations are allowed, the population at $t \gg T$ will be clonal, with all
 968 individuals having genome σ^{n_0} . Second, since the evolution is neutral and does not favour any genome in particular,
 969 the probability that σ^{n_0} is equal to a given genome σ is $1/N$. In other words, the probability that a genome at $t = 0$
 970 ultimately becomes the ancestor of all the future population is equal to its frequency in the $t = 0$ population.

971 We now try to find the genome σ that best predicts the future population on the long run, that is for $t \gg T$. Here,
 972 we take best to mean that the predictor minimizes $H(\sigma, \sigma^{n_0})$ where H is the Hamming distance defined by
 973

$$H(\sigma^a, \sigma^b) = \sum_{i=1}^L (1 - \delta_{\sigma_i^a, \sigma_i^b}), \quad (1)$$

974 with σ_i being the character appearing at position i of genome σ and δ the Kronecker delta. Since we do not know n_0 ,
 975 we have to average over all its possible values. σ must thus minimize the following quantity:

$$\begin{aligned} \langle H(\sigma, \sigma^{n_0}) \rangle_{n_0} &= \sum_{n=1}^N H(\sigma, \sigma^n) \\ &= \sum_{i=1}^L \sum_{n=1}^N (1 - \delta_{\sigma_i, \sigma_i^n}) \end{aligned} \quad (2)$$

by using the definition of the Hamming distance. We now assume that characters at each positions of the genomes can
 be indexed by an integer a running from 1 to q . For instance, if these were amino acid sequences, we could index the
 20 amino acids by a running from 1 to $q = 20$. We rewrite the Kronecker delta in the previous expression using this
 indexation:

$$\delta_{\sigma_i, \sigma_i^n} = \sum_{a=1}^q \delta_{\sigma_i, a} \delta_{\sigma_i^n, a}.$$

976 We also introduce the *profile* frequencies $p_i(a)$ of the population at time $t = 0$:

$$p_i(a) = \sum_{n=1}^N \delta_{\sigma_i^n, a}. \quad (3)$$

977 $p_i(a)$ represents the frequency at which character a appears at position i in genomes of the initial population.
 978 Equation 2 now becomes

$$\begin{aligned} \langle H(\sigma, \sigma^{n_0}) \rangle_{n_0} &= \sum_{i=1}^L \sum_{n=1}^N \left(1 - \sum_{a=1}^q \delta_{\sigma_i, a} \delta_{\sigma_i^n, a} \right) \\ &= \sum_{i=1}^L \left(1 - \sum_{a=1}^q \delta_{\sigma_i, a} p_i(a) \right) \\ &= \sum_{i=1}^L (1 - p_i(\sigma_i)) \end{aligned} \quad (4)$$

979 This means that the genome $\sigma = (\sigma_1 \dots \sigma_L)$ which best predicts the future population according to our definition is
 980 the one that minimizes the quantity $(1 - p_i(\sigma_i))$ for all positions i . This obviously implies that each σ_i must be chosen
 981 as to maximize $p_i(a)$, that is σ_i must be the character that appears the most frequently at position i . Thus, σ must be
 982 the *consensus* sequence of the initial population.

983 2. Predictor based on the local LBI maxima

In figure 15, we use several sequences as a predictor of the future population. Distance between two sets of sequences, *i.e.* the predictor sequences and the ones of the future population, is defined as the Earth Mover's Distance (EMD). Here, we show that for a population evolving under the same hypotheses as in section 1, the best *multiple* sequence long term predictor is again the consensus sequence with weight 1.

Let the predictor be a set of weighted sequences $\{(s^\alpha, q_\alpha)\}$. We again use the fact that in the long term, a unique sequence σ^{n_0} from the present will be the ancestor of the entire population. We want to compute the EMD from the predictor to σ^{n_0} , that is the EMD between the sets $\mathcal{X} = \{(s^\alpha, q_\alpha)\}$ and $\mathcal{Y} = \{\sigma^{n_0}, 1\}$. Applying the definition of the Methods section, it follows that the weights \mathbf{w} are in this case equal to the q_α s. By averaging over all values of n_0 , we now obtain

$$\langle \text{EMD}(\{(s^\alpha, q_\alpha)\}) \rangle_{n_0} = \sum_{n=1}^N \sum_{\alpha} H(s^\alpha, \sigma^n) \cdot q_\alpha.$$

By the same calculation procedure as in the previous section, this expression simplifies to

$$\langle \text{EMD}(\{(s^\alpha, q_\alpha)\}) \rangle_{n_0} = \sum_{i=1}^L \left(1 - \sum_{a=1}^q p_i(a) q_i(a) \right),$$

where the profile of the present population $p_i(a)$ has already been defined, and $q_i(a)$ stands for the profile of the predictor, that is

$$q_i(a) = \sum_{\alpha} \delta_{s_i^\alpha, a} q_\alpha.$$

984 To minimize this distance, we find a profile $q_i(a)$ that maximizes the quantity $\sum_{\alpha} \delta_{s_i^\alpha, a} q_\alpha$ for each position i . It is
 985 clear that this is done by assigning a value $q_i(a) = 1$ if a maximizes $p_i(a)$, and $q_i(a) = 0$ otherwise. Thus, the profile of
 986 the predictor must be that of the consensus sequence, which is only possible if the predictor becomes $\{\sigma^{cons}, 1\}$.

987 3. Biases in frequency estimations

988 The frequency of mutations in a given time-bin is simply performed by computing their frequency in sequences
 989 sampled in that time bin. This leads to potential biases in estimating frequencies, that arise for two reasons:

- 990 (i) A mutation present at frequency p in the population might be observed at another frequency $f \neq p$ if f is
 991 estimated using a sub-sample of the population.
- 992 (ii) For a neutrally evolving population, the distribution of frequencies of alleles is of the form $P(p) \propto 1/p$. This
 993 means that the amount of alleles at frequency p is lower when p is higher.

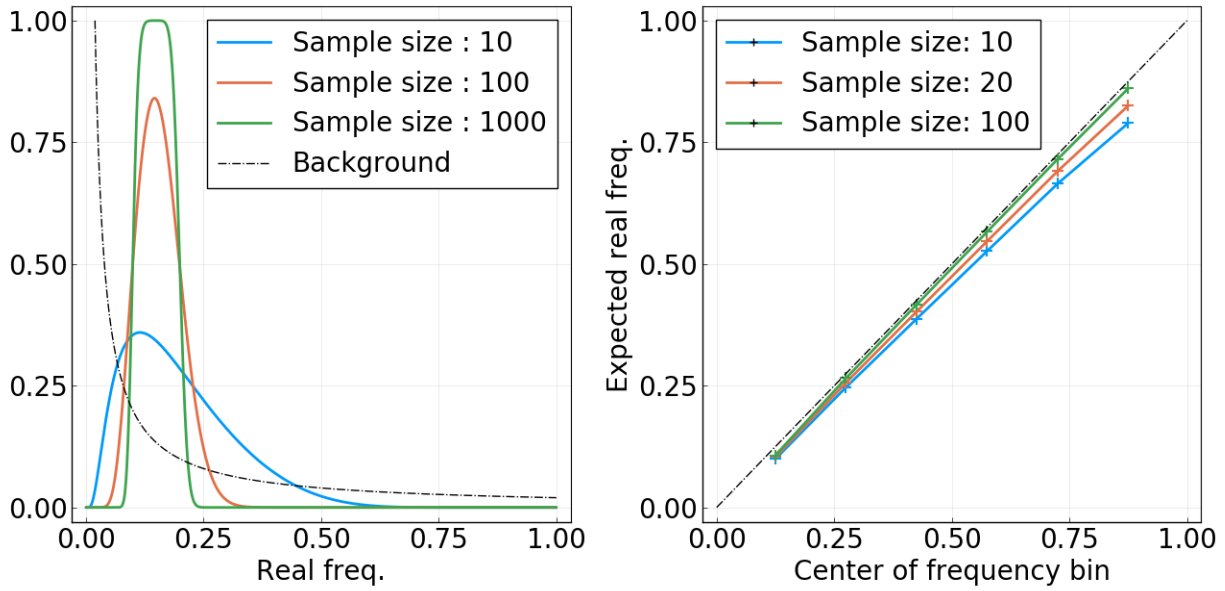


Figure S 1. **Left:** For a mutation present at frequency p in the population, probability of being observed in the frequency bin $[0.1, 0.2]$ as a function of p and for different sample sizes n . The dashed black line sketches the (non-normalized) background distribution $P_b(p)$. **Right:** Expected “real” average frequency of mutations found in frequency bin $[f_1, f_2]$ as a function of the centre of the bin $(f_1 + f_2)/2$, for different sample sizes.

994 To illustrate (i), let us compute the probability that a mutation present at “real” frequency p in the population is
 995 found to be in a given frequency bin $[f_1, f_2]$ when p is estimated from a sample of size n . The sample consists of n
 996 observations $\{x_i\}$ with $1 \leq i \leq n$, with $x_i = 1$ if sequence sequence i of the sample bears the mutation, and $x_i = 0$ if
 997 not. If n is small with regard to the total population size, we can consider the x_i as random variables with a binomial
 998 distribution, meaning that $P(x_i = 1) = p$ and $P(x_i = 0) = 1 - p$. The empirical frequency f is then estimated by
 999 taking the average of the x_i variables, that is $f = (x_1 + \dots + x_n)/n$. If those are independently sampled and n is large
 1000 enough, the probability of measuring value f is given by the Central Limit Theorem:

$$P_{n,p}(f) \propto e^{-(f-p)^2/2\sigma^2}, \quad \text{where } \sigma^2 = \frac{p(1-p)}{n}. \quad (5)$$

1001 To compute the probability that this mutation is found in a given frequency bin $[f_1, f_2]$, we integrate this distribution:

$$P_{f_1, f_2}(p, n) = \int_{f_1}^{f_2} dx P_{n,p}(x). \quad (6)$$

1003 Function $P_{f_1, f_2}(p, n)$ is shown as a function of p for a fixed interval and for different values of n in the first panel of
 1004 figure S1. Note the asymmetry of it: the variance of a binomial distribution of parameter p is small when p is close to
 1005 0 or 1, and goes through a maximum at $p = 0.5$. For this reason, mutations present at frequency p close to 0.5 have a
 1006 higher probability of being observed in other frequency bins. On the contrary, this is unlikely for very rare or very
 1007 frequent mutations.
 1008

1009 We now try to estimate biases in frequency estimation due this phenomenon. Given a set of mutations that have
 1010 been measured in frequency bin $[f_1, f_2]$, what is the average *real* frequency of these mutations? To compute this, we
 1011 need to sum $P_{f_1, f_2}(p, n)$ over all possible real frequencies p , giving us the amount of mutations that are observed in
 1012 interval $[f_1, f_2]$, and weigh this sum by the frequency value p as well as by the background distribution of frequencies
 1013 $P_b(p) \propto 1/p$. This last quantity represents the expected amount of mutations that are present at frequency p in the
 1014 population. Note that there is no divergence problem as the smallest non zero frequency is $1/N$, where N is the
 1015 population size. This leads us to the following expression for the average of “real” frequencies:

$$\begin{aligned} \langle p \rangle(f_1, f_2, n) &= \int_{1/N}^{1-1/N} dp P_{f_1, f_2}(p, n) P_b(p) p \\ &= \int_{1/N}^{1-1/N} dp P_{f_1, f_2}(p, n). \end{aligned} \quad (7)$$

1016 We have not made normalization explicit in these equations. It is simply achieved by dividing the above expression by
1017 $\int dp P_{f_1, f_2}(p, n) P_b(p)$.
1018 In the second panel of figure S1, $\langle p \rangle(f_1, f_2, n)$ is plotted as a function of the centre of the interval $[f_1, f_2]$ and for
1019 different values of n . For sample sizes $n > 100$, the biases due to this effect are almost non-existent. For smaller
1020 samples, for instance $n = 10$, they are small but non-negligible. However, we argue that this is not a significant problem
1021 with respect to the main results presented in this article. First, figure S6 shows that sample sizes of the order of $n = 10$
1022 are only the case for a few months in the period going from year 2000 to 2018. From 2010 and onwards, more than a
1023 hundred sequences are available per month for most months. Secondly, even if most samples were in the $n = 10$ case,
1024 deviations shown in figure S1 are small enough that results shown in figures 2 and 3 would be *qualitatively* unchanged.
1025 Note that using the centre of the interval as a reference in figure S1, *i.e.* $(f_1 + f_2)/2$, would be correct in the case of
1026 a very large n and a flat background distribution $P_b(p)$. For figures 2 and 3 of the main text however, the average
1027 frequency of mutations found in an interval $[f_1, f_2]$ is computed by taking the average of the observed frequencies, and
1028 not the centre of the interval. This partially takes into account biases considered here, as the background distribution
1029 $P_b(p)$ is then accounted for, even though it is equivalent to assuming infinite sample sizes.

1030

4. Cutting off the HA1 159S branch

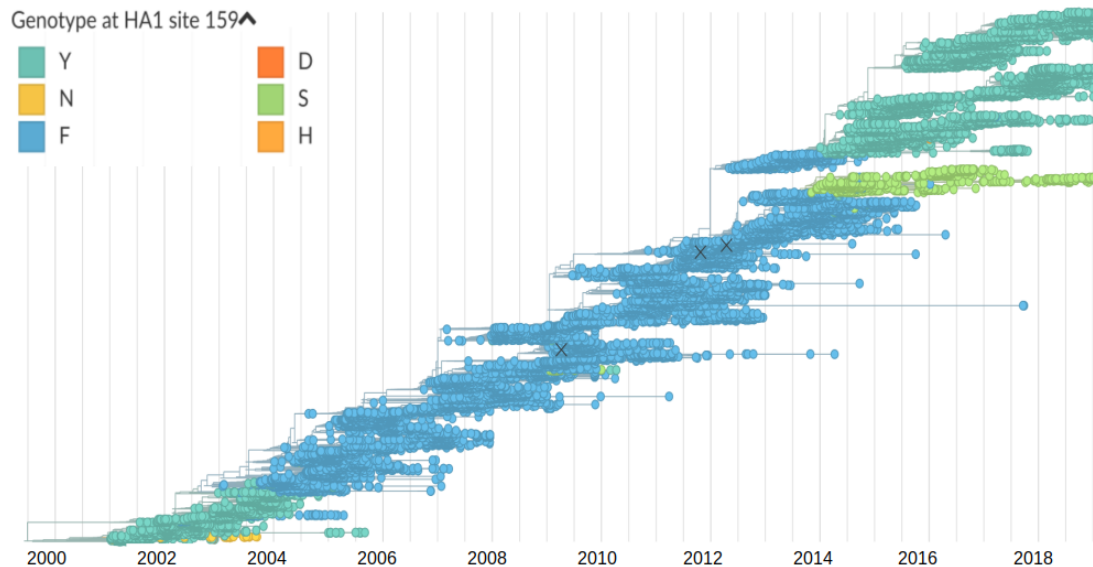


Figure S 2. Tree used for this study, based on a random selection of 100 strains per month from year 2002 to 2018. Nodes and branches are colored according to the amino acid found at position HA1:159. The HA1 159S mutation is visible as a thin but long light-green color branch, coalescing with the “trunk” around year 2013.

1031 The analysis of the main text is in a large part based on the probability of fixation of mutations. The motivation
1032 underlying this choice is the relatively short coalescence time of the A/H3N2 influenza population, typically around
1033 three years. This can be seen in figure 2 of the main text, which shows the typical lifetime of frequency trajectories,
1034 ending in fixation or loss after at most 3 years in most cases. The tree in figure S2 is another illustration of this: for
1035 the most part of it, a “trunk” is clearly identifiable, and lineages that depart from it have a relatively short lifetime.
1036 This is no longer the case since the year ~ 2013 : two clades have been competing since then, with no definite way to
1037 identify a trunk in the tree. The clade defined by the HA1 159S mutation, colored in light green on figure S2, is one of
1038 these two competing lineages. Because of this particular situation, the number of mutations fixating in the population
1039 is strongly reduced, as a mutation must appear in both clades to reach a frequency of 1. This is a potential flaw in our
1040 analysis, which concentrates on mutations fixating.

1041 For this reason, we decided to re-run our analysis after having cut off the HA1 159S clade. In other words, we remove
1042 from the set of sequences those that carry the HA1 159S mutation. Results are shown in figures , equivalent to figures 2
1043 and 3 of the main text. It is clear that qualitative results are left unchanged when this competing clade is removed.
1044 This can be surprising, as almost no complete fixation of an amino acid mutation has occurred since 2013. Cutting off
1045 the HA1 159S branch should thus result in many new fixations, changing the analysis. The reason for the similarity
1046 of results can be explained: fixation (resp. loss) of a mutation are defined here as the frequency of this mutation
1047 being measured above 95% (resp. 5%) frequency for two months in a row. As the HA1 159S clade is rather sparsely
1048 populated, it reaches frequencies lower than 5% two times (in 2015 and 2017), allowing mutations in the competing
1049 clade to “fix” as defined here. Thus, removing strains carrying HA1 159S does not introduce a significant amount of
1050 “new” fixation events.

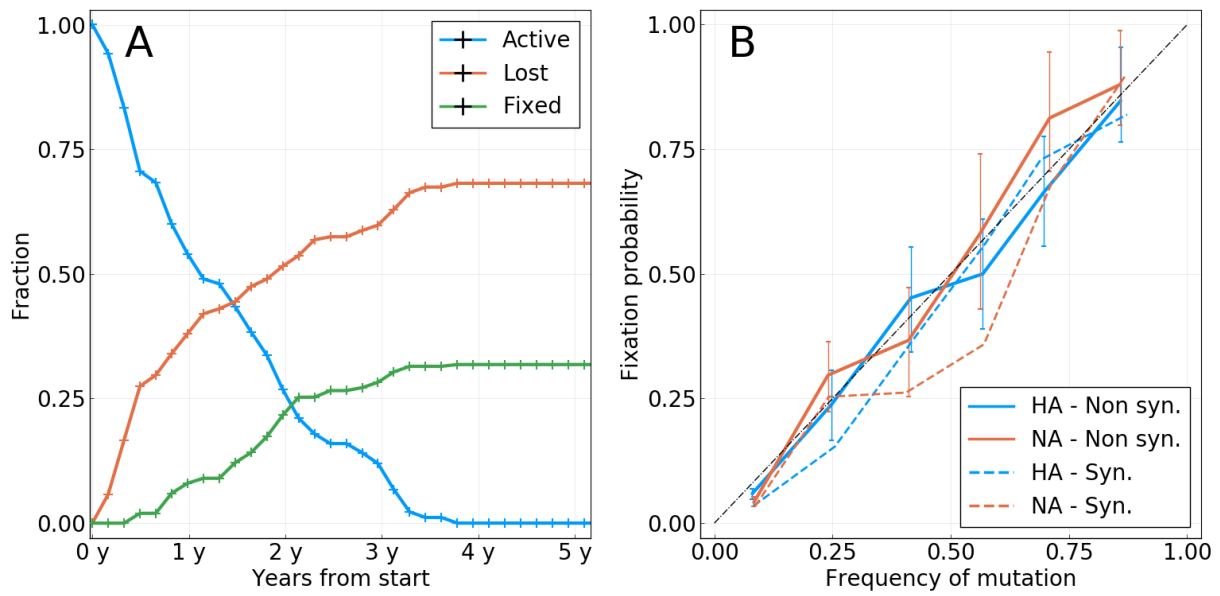


Figure S 3. Equivalent to figure 2 of the main text, but with strains carrying the HA1 159S mutation removed.

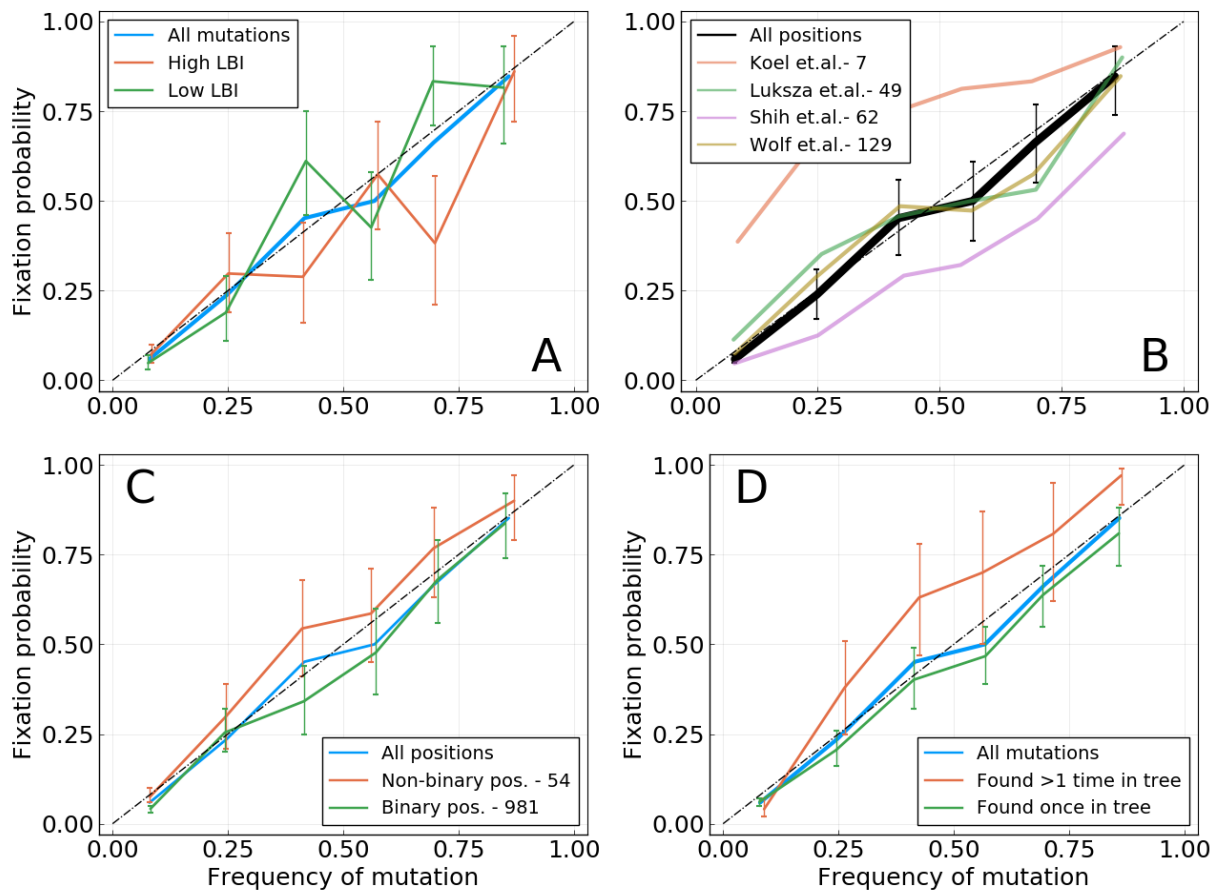


Figure S 4. Equivalent to figure 3 of the main text, but with strains carrying the HA1 159S mutation removed.

1051

5. Probability of fixation in single locus model of evolution

1052
1053
1054

In [18], Kimura investigates a simple model of evolution with a single locus and a population of size N . In this framework, a mutation at this locus with fitness effect s and observed at frequency f has the following probability of fixation:

$$P_{fix}(f|s, N) = \frac{1 - e^{-sNf}}{1 - e^{-sN}}. \quad (8)$$

1055 Expanding this formula for $sN \ll 1$, that is in the weak selection regime, yields at the first order

$$P_{fix}(f|s, N) = f + f(1 - f) \frac{sN}{2}. \quad (9)$$

1056
1057
1058
1059
1060
1061

Equation 9 tells us two things. First, when the mutation is neutral, that is $s = 0$, we have $P_{fix}(f) = f$. This naturally confirms the result obtained for a neutral model of evolution. Second, when $sN \neq 0$, we can expect deviations from the diagonal in a P_{fix} against f plot. The sign of these deviations is determined by the sign of s , with beneficial mutations being found above diagonal while deleterious one are found below. The amplitude of these deviations depends on the strength of selection sN , as well as on the frequency through the $f(1 - f)$ term, making them larger for $f \sim 0.5$.

6. Mutation tables

Gene	Position	AA	Start date	End date	Shih	Luksza	Koel	Tree counts
HA1	144	D	2001-06-09	2002-02-04	true	true	false	0
HA1	189	N	2003-07-29	2004-05-24	false	true	true	2
HA1	159	F	2003-08-28	2004-05-24	false	true	true	2
HA1	226	I	2003-09-27	2004-09-21	true	true	false	3
HA1	145	N	2003-12-26	2004-11-20	false	true	true	2
HA1	227	P	2003-05-30	2005-04-19	false	true	false	2
HA2	32	I	2004-06-23	2005-07-18	false	false	false	1
HA1	193	F	2004-12-20	2006-03-15	false	true	true	1
HA2	46	D	2006-06-13	2007-05-09	false	false	false	2
HA2	121	K	2006-06-13	2007-06-08	false	false	false	1
HA1	50	E	2006-09-11	2007-06-08	false	true	false	2
HA1	140	I	2006-11-10	2007-11-05	true	false	false	1
HA1	173	Q	2007-07-08	2009-01-28	true	true	false	2
HA2	32	R	2007-07-08	2009-01-28	false	false	false	1
HA1	158	N	2009-01-28	2009-07-27	true	true	true	2
HA1	189	K	2009-01-28	2009-07-27	false	true	true	2
HA1	212	A	2009-03-29	2011-01-18	false	false	false	2
HA1	45	N	2010-03-24	2013-02-06	false	false	false	3
HA1	223	I	2010-12-19	2013-02-06	false	false	false	2
HA1	48	I	2011-03-19	2013-02-06	false	false	false	1
HA1	198	S	2011-03-19	2013-02-06	false	false	false	1
HA1	312	S	2009-08-26	2013-03-08	false	false	false	3
HA1	278	K	2011-06-17	2013-03-08	false	true	false	1
HA1	145	S	2011-04-18	2013-04-07	false	true	true	4
HA1	33	R	2011-06-17	2013-06-06	false	false	false	2
HA2	160	N	2012-07-11	2015-09-24	false	false	false	3
HA1	225	D	2013-08-05	2015-09-24	false	false	false	3
HA1	3	I	2013-08-05	2016-11-17	false	false	false	2
HA1	159	Y	2014-02-01	2016-11-17	false	true	true	2
HA1	160	T	2014-01-02	2017-07-15	false	true	false	2

Table S I. The 30 trajectories that took place between year 2000 and year 2018 and resulted in fixation. Columns **Shih**, **Luksza** and **Koel** respectively indicate whether the position is found in the epitopes lists in (respectively) [3], [11] and [5]. The **Tree counts** column indicates the number of times the mutation corresponding to the trajectory can be found in the phylogenetic tree. Note that a trajectory is only shown in the table if the sequenced population counts more than 10 strains at its time of fixation. This explains that only 30 trajectories are displayed, whereas more mutations did fix in this period of time.

Gene	Position	AA	Start date	End date	Fixation	Max. freq.
HA1	106	A	2001-02-09	2002-02-04	lost	1.0
HA1	144	D	2001-06-09	2002-02-04	fixed	1.0
HA1	105	H	2003-04-30	2003-10-27	lost	1.0
HA1	126	D	2003-04-30	2004-05-24	lost	1.0
HA1	140	Q	2004-01-25	2004-06-23	lost	0.31
HA1	226	I	2003-09-27	2004-09-21	fixed	1.0
HA1	173	E	2004-12-20	2006-03-15	lost	0.63
HA1	142	G	2006-06-13	2007-05-09	lost	0.71
HA1	144	D	2006-07-13	2007-05-09	lost	0.67
HA1	128	A	2006-09-11	2007-05-09	lost	0.25
HA1	157	S	2006-09-11	2007-05-09	lost	0.59
HA1	140	I	2006-11-10	2007-11-05	fixed	1.0
HA1	173	N	2007-12-05	2008-07-02	lost	0.3
HA1	157	S	2007-12-05	2008-09-30	lost	0.31
HA1	173	E	2006-06-13	2008-12-29	lost	0.67
HA1	173	Q	2007-07-08	2009-01-28	fixed	0.96
HA1	158	N	2009-01-28	2009-07-27	fixed	0.96
HA1	62	K	2009-01-28	2011-05-18	lost	0.73
HA1	144	K	2009-01-28	2011-05-18	lost	0.75
HA1	62	V	2011-04-18	2011-09-15	lost	0.34
HA1	157	S	2013-05-07	2015-09-24	lost	0.35
HA1	128	A	2012-08-10	2016-11-17	lost	0.81
HA1	197	K	2015-11-23	2016-11-17	lost	0.27
HA1	142	R	2018-05-11	2018-10-08	lost	0.38
HA1	142	G	2012-03-13		poly	0.86
HA1	144	S	2013-12-03		poly	0.96
HA1	121	K	2015-12-23		poly	0.82
HA1	142	K	2016-05-21		poly	0.77
HA1	62	G	2017-03-17		poly	0.75
HA1	128	A	2018-01-11		poly	0.56

Table S II. Trajectories of mutations at epitope positions in [3] (*Shih et. al.*) that have been observed at least once above frequency 0.25. The **Fixation** column indicates whether the mutation has fixed, disappeared, or is still polymorphic as of October 2018. The **Max.freq.** column indicates the maximum frequency reached by the trajectory. A maximum frequency of 1 for mutations that finally disappear is explained by trajectories reaching frequency 1 for one time bin and going back to lower values for following ones (a frequency above 0.95 for two time bins in a row defines fixation).

Gene	Position	AA	Start date	End date	Fixation	Max. freq.
HA1	50	G	2001-02-09	2002-02-04	lost	1.0
HA1	144	D	2001-06-09	2002-02-04	fixed	1.0
HA1	126	D	2003-04-30	2004-05-24	lost	1.0
HA1	189	N	2003-07-29	2004-05-24	fixed	1.0
HA1	159	F	2003-08-28	2004-05-24	fixed	1.0
HA1	226	I	2003-09-27	2004-09-21	fixed	1.0
HA1	145	N	2003-12-26	2004-11-20	fixed	1.0
HA1	188	N	2004-07-23	2005-02-18	lost	0.36
HA1	227	P	2003-05-30	2005-04-19	fixed	1.0
HA1	173	E	2004-12-20	2006-03-15	lost	0.63
HA1	193	F	2004-12-20	2006-03-15	fixed	0.97
HA1	142	G	2006-06-13	2007-05-09	lost	0.71
HA1	144	D	2006-07-13	2007-05-09	lost	0.67
HA1	157	S	2006-09-11	2007-05-09	lost	0.59
HA1	50	E	2006-09-11	2007-06-08	fixed	0.95
HA1	173	N	2007-12-05	2008-07-02	lost	0.3
HA1	157	S	2007-12-05	2008-09-30	lost	0.31
HA1	173	E	2006-06-13	2008-12-29	lost	0.67
HA1	173	Q	2007-07-08	2009-01-28	fixed	0.96
HA1	158	N	2009-01-28	2009-07-27	fixed	0.96
HA1	189	K	2009-01-28	2009-07-27	fixed	0.96
HA1	213	A	2009-01-28	2010-02-22	lost	0.68
HA1	144	K	2009-01-28	2011-05-18	lost	0.75
HA1	53	N	2009-11-24	2013-02-06	lost	0.72
HA1	278	K	2011-06-17	2013-03-08	fixed	0.98
HA1	145	S	2011-04-18	2013-04-07	fixed	0.99
HA1	159	S	2013-11-03	2015-08-25	lost	0.46
HA1	157	S	2013-05-07	2015-09-24	lost	0.35
HA1	159	Y	2014-02-01	2016-11-17	fixed	0.97
HA1	159	S	2015-10-24	2016-11-17	lost	0.4
HA1	197	K	2015-11-23	2016-11-17	lost	0.27
HA1	160	T	2014-01-02	2017-07-15	fixed	0.96
HA1	142	R	2018-05-11	2018-10-08	lost	0.38
HA1	135	N	2018-06-10	2018-10-08	lost	0.38
HA1	142	G	2012-03-13		poly	0.86
HA1	144	S	2013-12-03		poly	0.96
HA1	121	K	2015-12-23		poly	0.82
HA1	142	K	2016-05-21		poly	0.77
HA1	131	K	2016-09-18		poly	0.77
HA1	135	K	2016-11-17		poly	0.47

Table S III. Same as table SII, for [11] (*Luksza et. al.*).

Gene	Position	AA	Start date	End date	Fixation	Max. freq.
HA1	189	N	2003-07-29	2004-05-24	fixed	1.0
HA1	159	F	2003-08-28	2004-05-24	fixed	1.0
HA1	145	N	2003-12-26	2004-11-20	fixed	1.0
HA1	193	F	2004-12-20	2006-03-15	fixed	0.97
HA1	158	N	2009-01-28	2009-07-27	fixed	0.96
HA1	189	K	2009-01-28	2009-07-27	fixed	0.96
HA1	145	S	2011-04-18	2013-04-07	fixed	0.99
HA1	159	S	2013-11-03	2015-08-25	lost	0.46
HA1	159	Y	2014-02-01	2016-11-17	fixed	0.97
HA1	159	S	2015-10-24	2016-11-17	lost	0.4

Table S IV. Same as table SII, for [5] (*Koel et. al.*).

1063

7. Supplementary figures

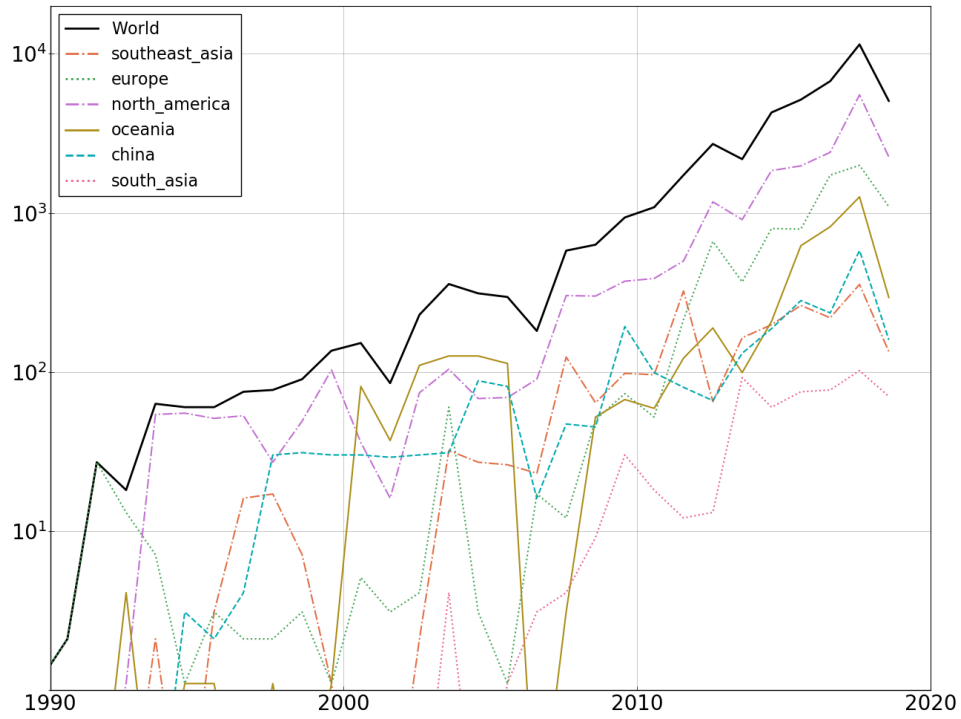


Figure S 5. Number of A/H3N2 HA sequences per year from year 1990.

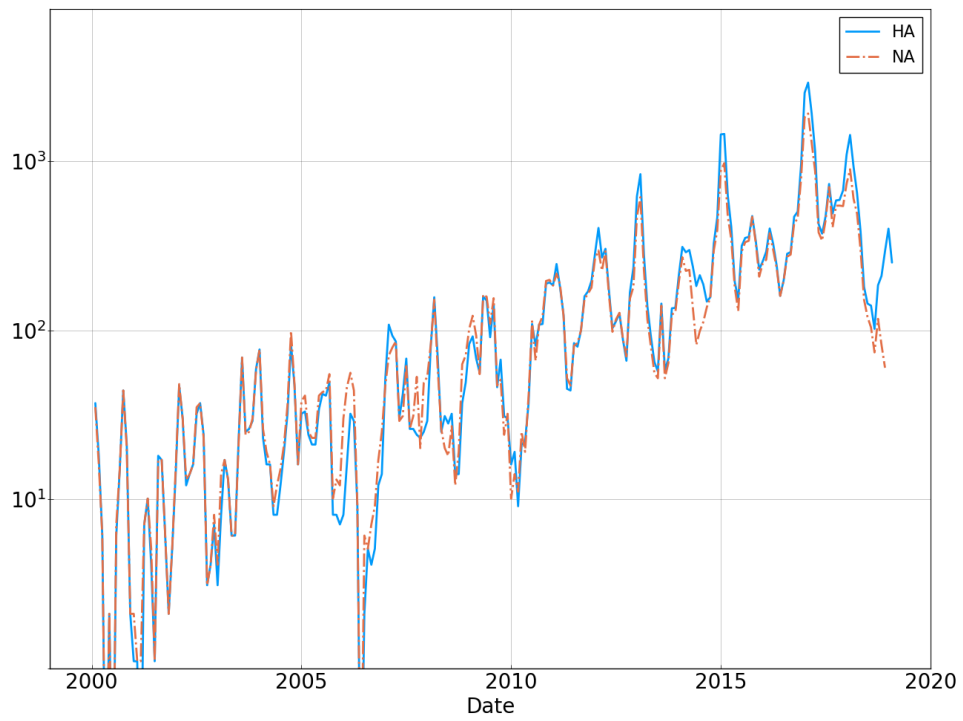


Figure S 6. Number of H3N2 HA and NA sequences per month from year 2000.

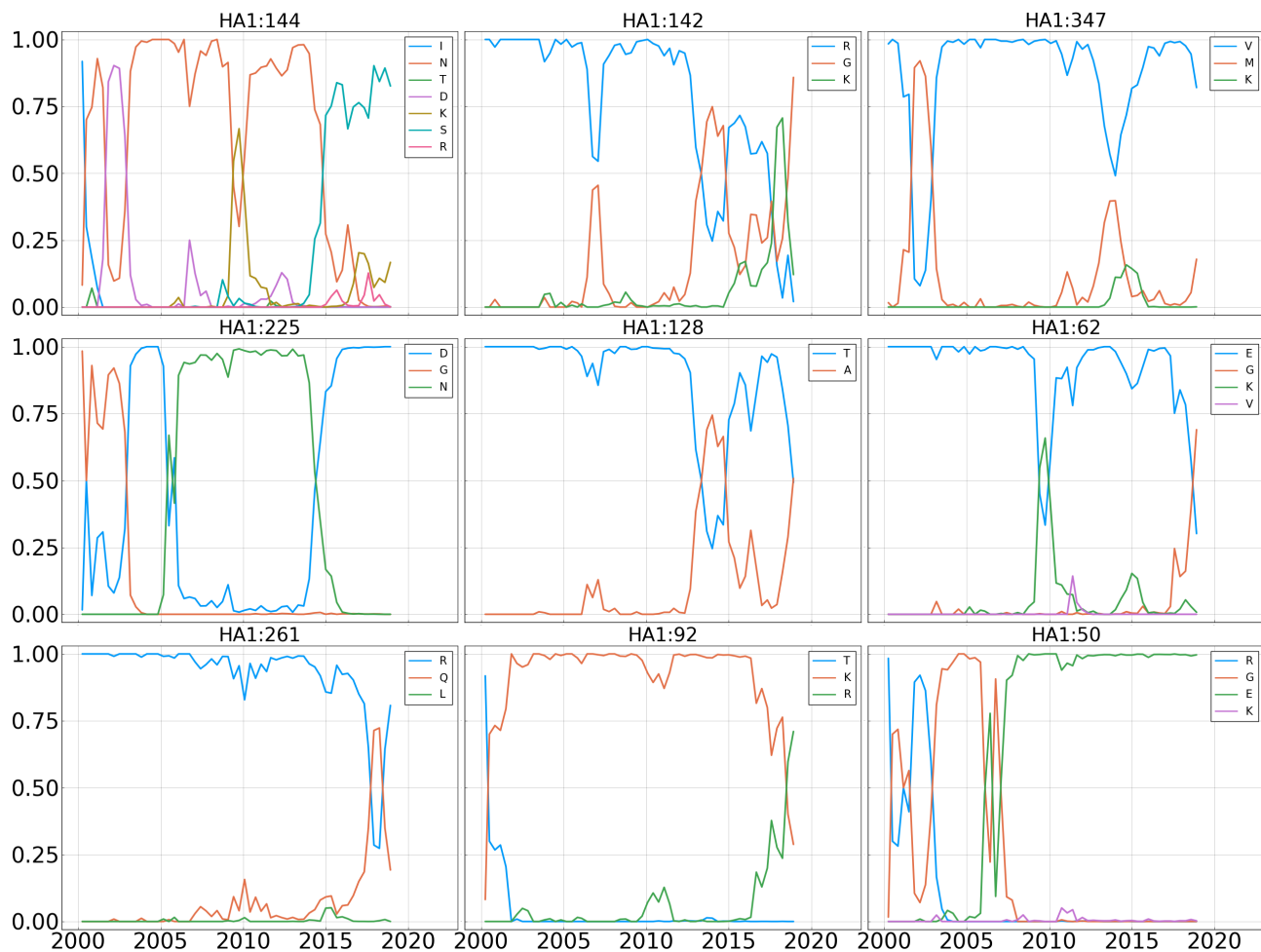


Figure S 7. Frequency trajectories for the 9 most entropic positions in the A/H3N2 HA protein.

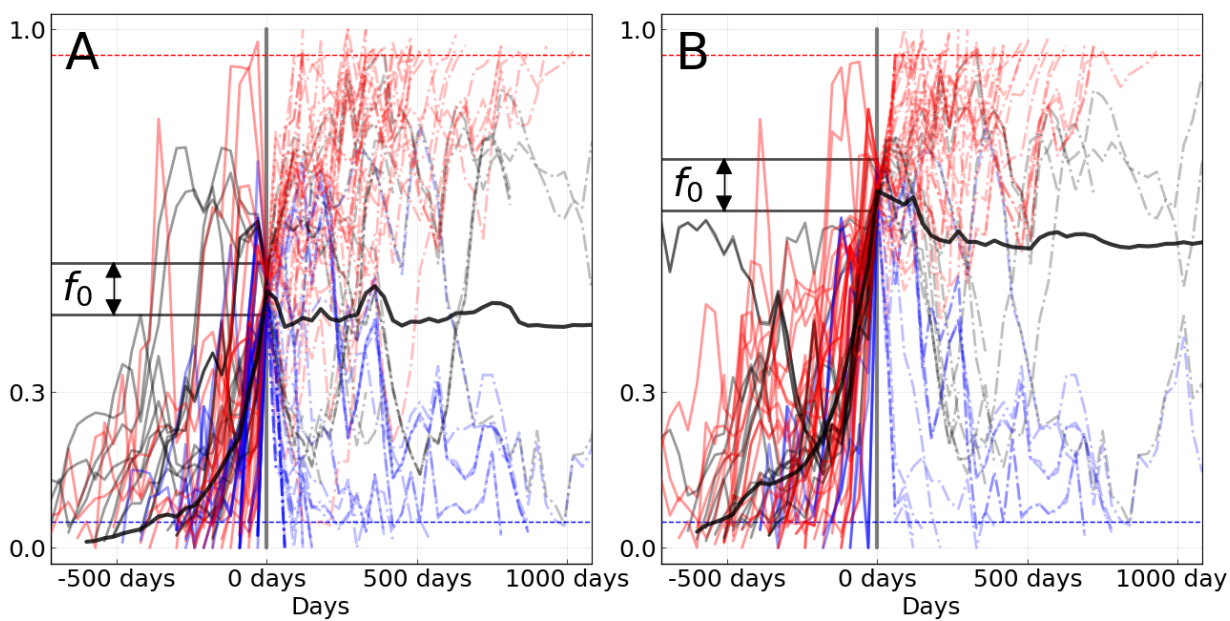


Figure S 8. Equivalent to panel **B** of figure 1 of the main text for A/H3N2, with f_0 equal 0.5 in **A** (76 trajectories), and 0.7 in **B** (63 trajectories).

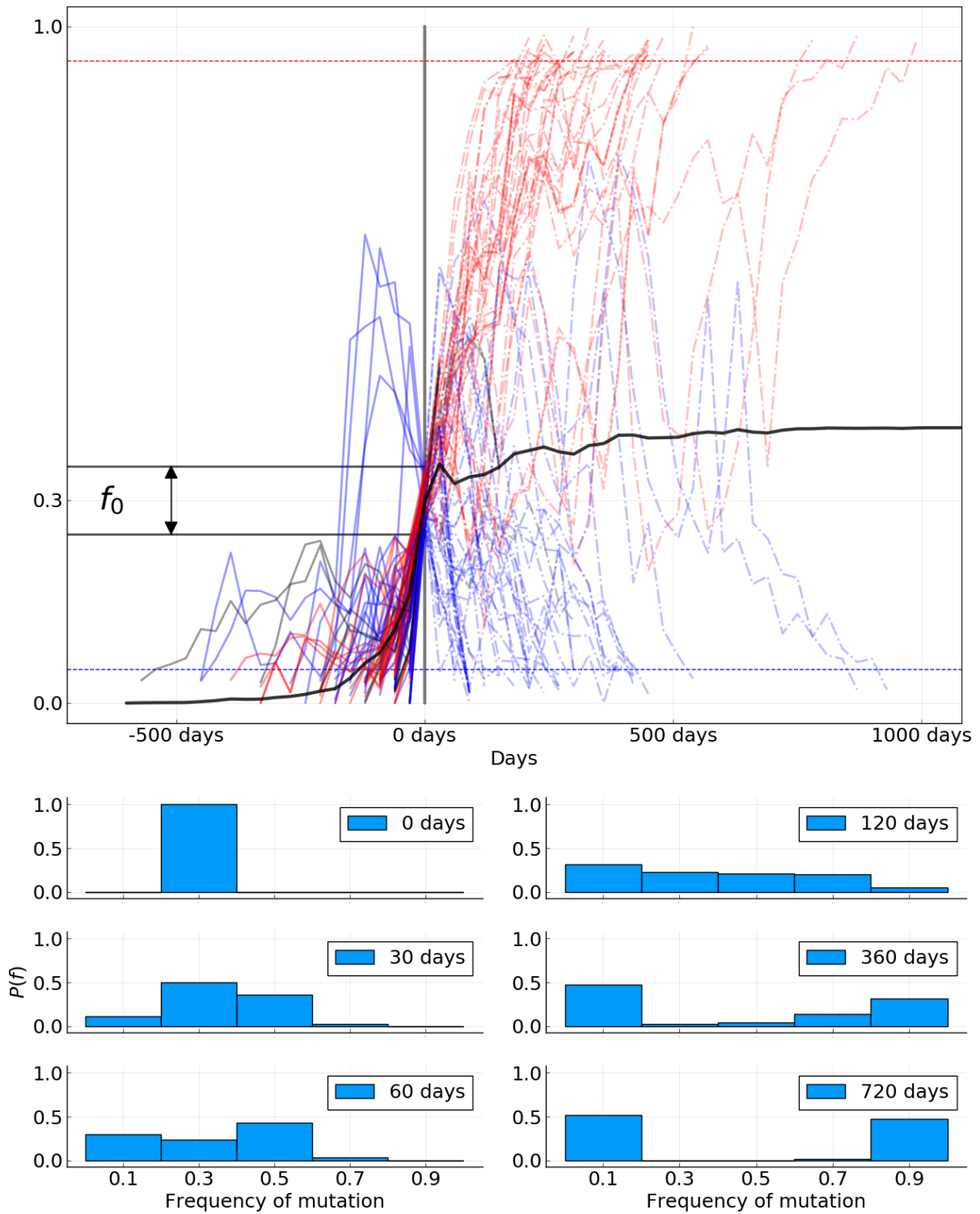


Figure S 9. Equivalent to panels B and C of figure 1 of the main text for A/H1N1pdm influenza. 89 trajectories are shown and participate to the mean (thick black line).

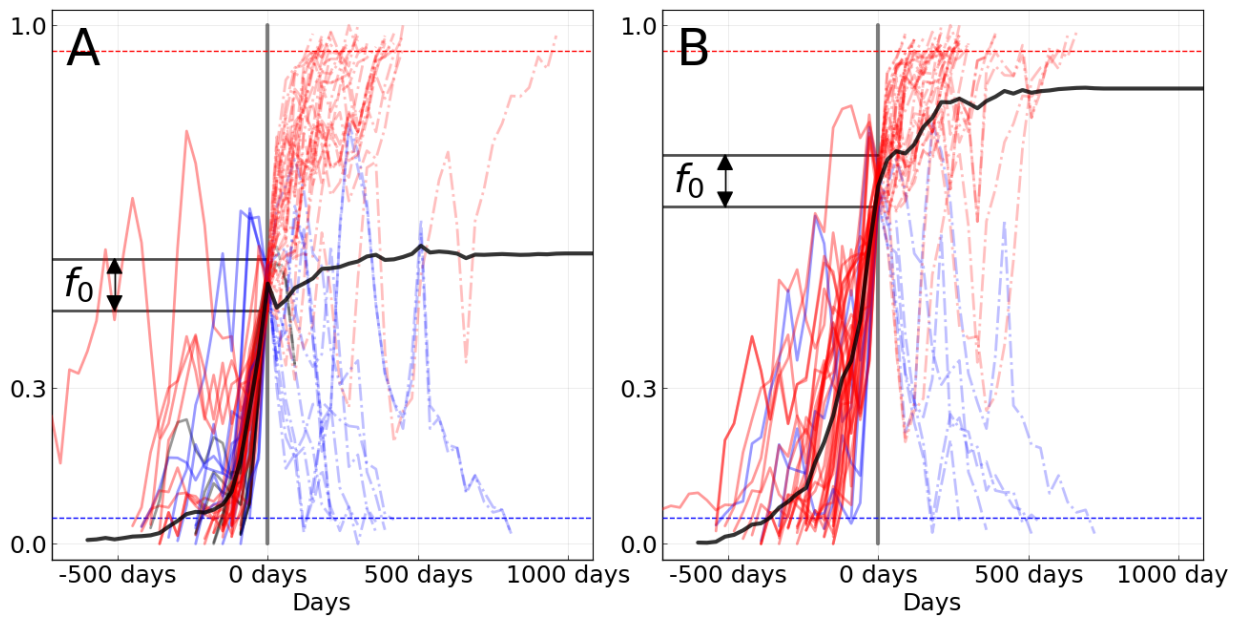


Figure S 10. Equivalent to panel **B** of figure 1 of the main text for A/H1N1pdm, with f_0 equal 0.5 in **A** (50 trajectories), and 0.7 in **B** (41 trajectories).

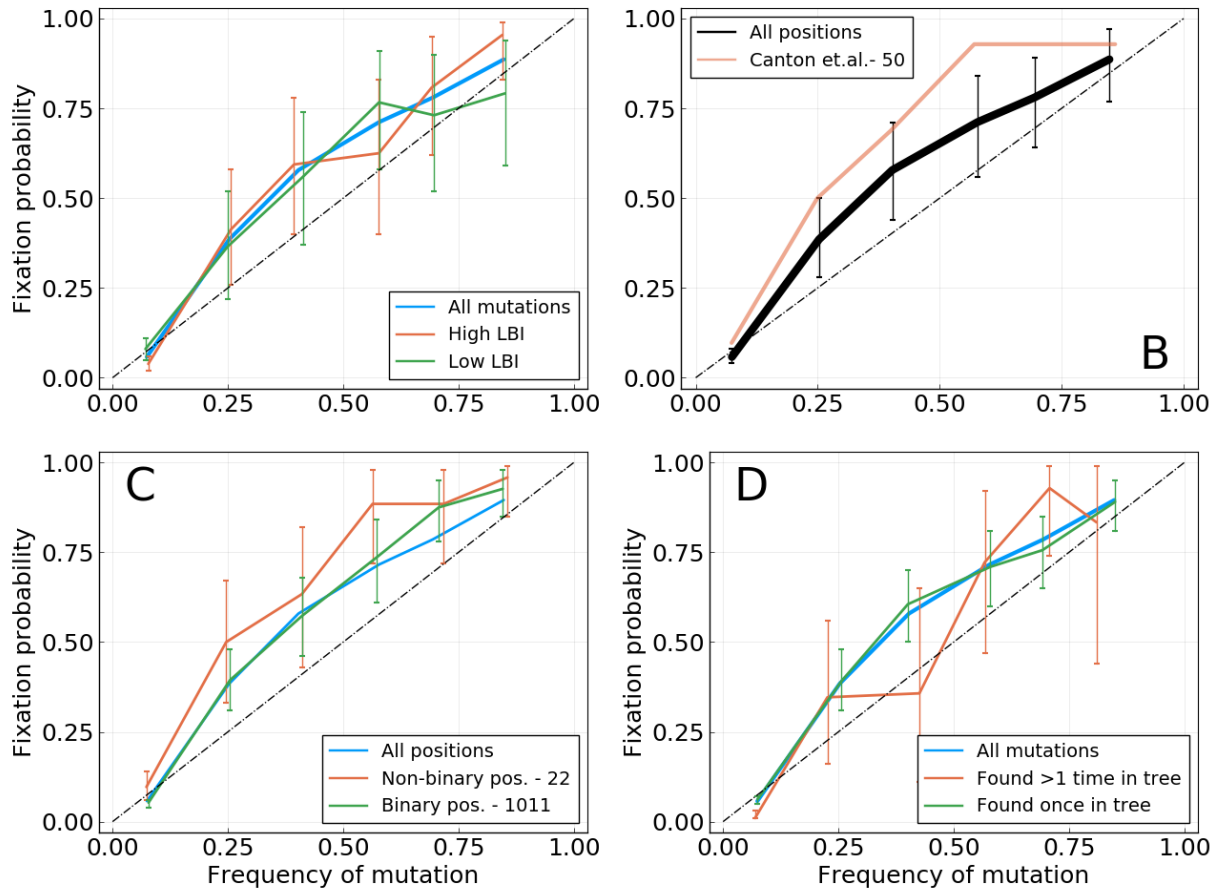


Figure S 11. Equivalent of figure 3 of the main text for the HA gene of A/H1N1pdm influenza. Fixation probability $P_{fix}(f)$ as a function of frequency. **A:** Mutation with higher or lower LBI values, based on their position with respect to the median LBI value. **B:** Different lists of epitope positions in the HA protein. The authors and the number of positions is indicated in the legend. **C:** Mutations for binary positions, *i.e.* positions for which we never see more than two amino acids in the same time bin. **D:** Mutations that appear once or more than once in the tree for a given time bin.

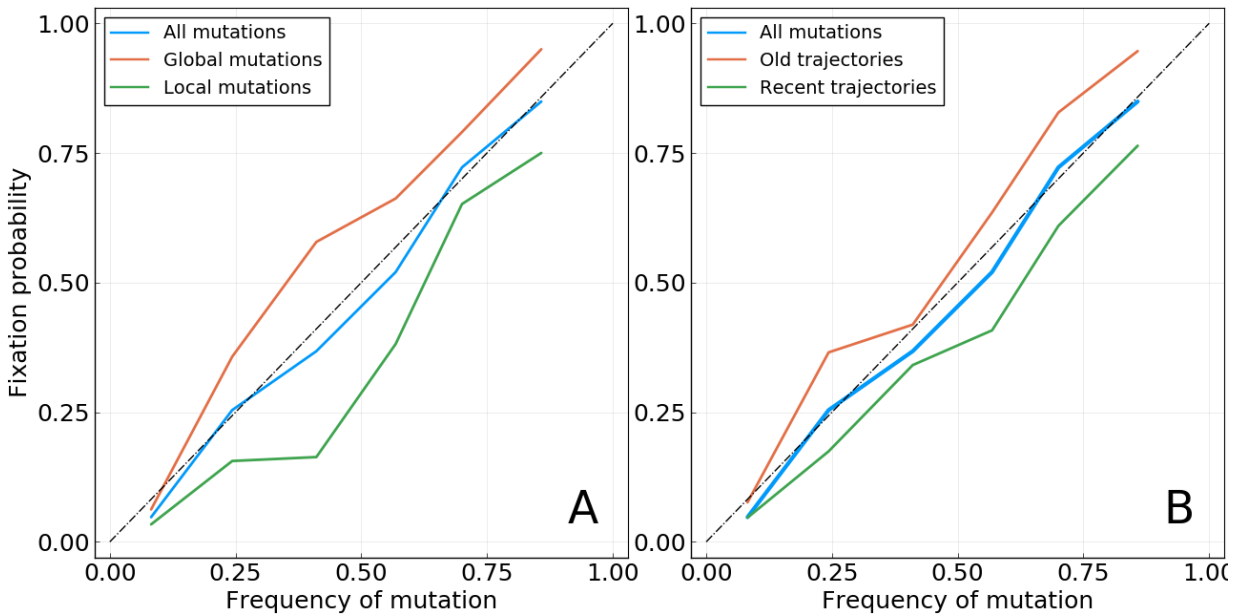


Figure S 12. Based on A/H3N2 HA and NA. **A**: Mutations with a higher or lower geographical spread, based on the median value of the score used (see Methods). *Note*: the words *local* and *global* only reflect the position of the geographic spread of the mutation relative to the median value computed for all mutations found at this frequency. As this median value may change with the considered frequency bin, so does the definition of local and global mutations. **B**: Mutations whose trajectories are older or more recent, based on the median age of trajectories when reaching the considered frequency f .

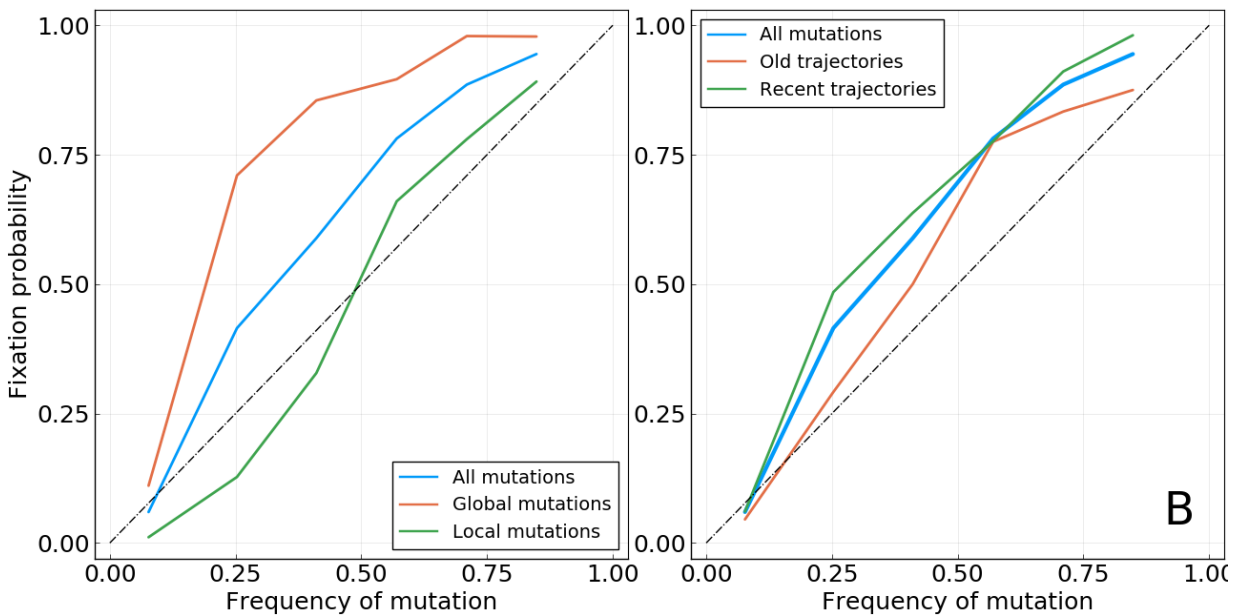


Figure S 13. Based on A/H1N1pdm HA and NA. **A**: Mutations with a higher or lower geographical spread, based on the median value of the score used (see Methods). *Note*: the words *local* and *global* only reflect the position of the geographic spread of the mutation relative to the median value computed for all mutations found at this frequency. As this median value may change with the considered frequency bin, so does the definition of local and global mutations. **B**: Mutations whose trajectories are older or more recent, based on the median age of trajectories when reaching the considered frequency f .

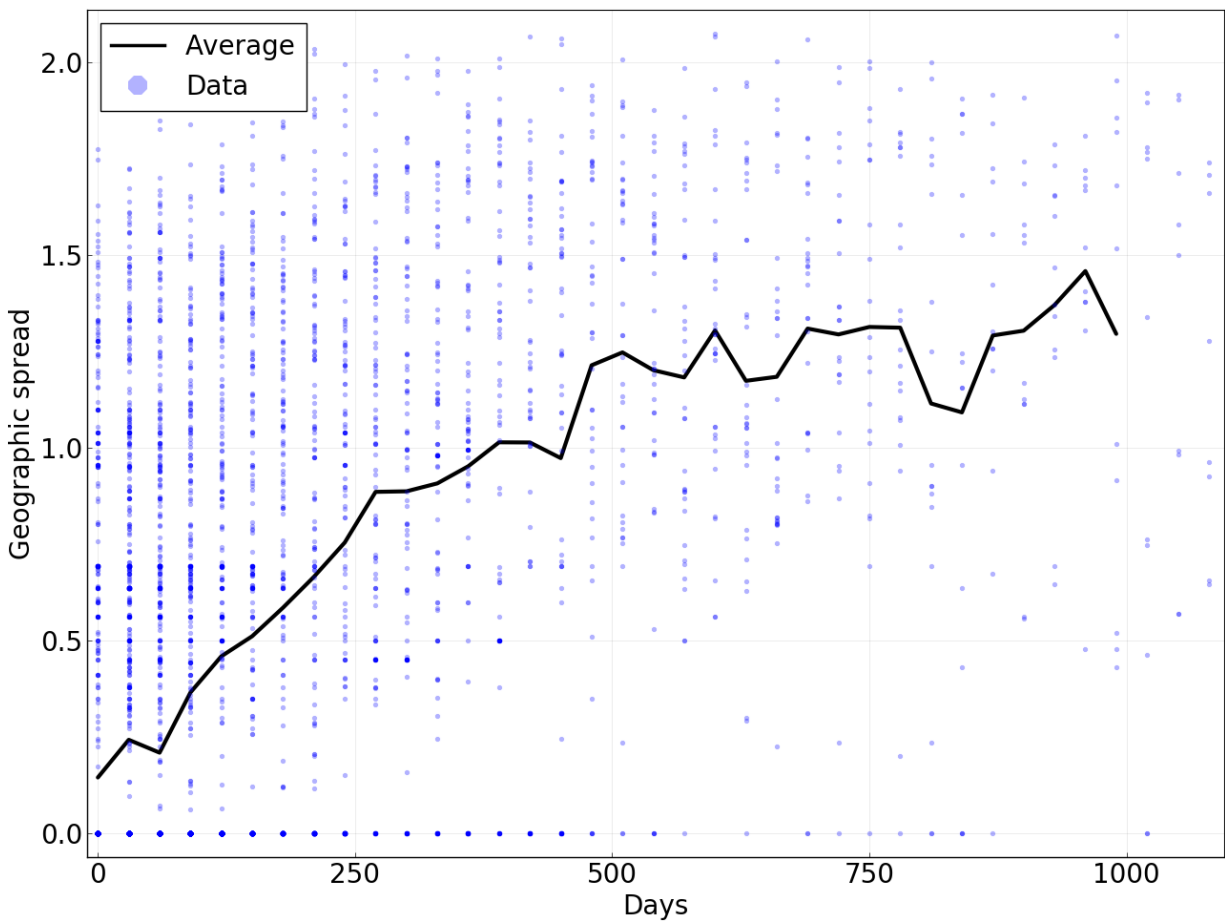


Figure S 14. Geographic spread of mutations as a function of the time for which they have been present in the population above a frequency of 5%. Points represent individual mutations and for a population in a given time bin. The line is the average of dots for a given value on the x -axis. Based on data for A/H3N2 HA.

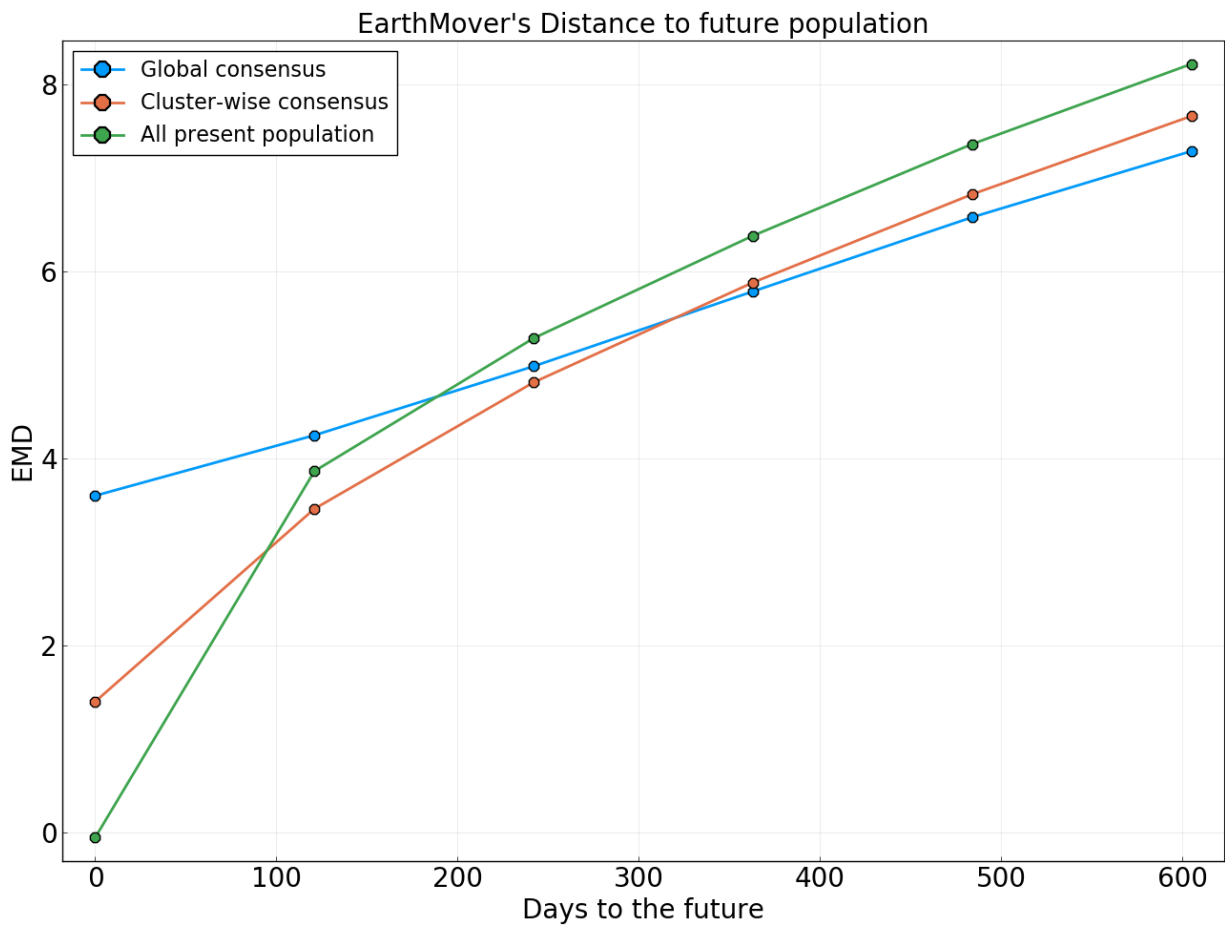


Figure S 15. Earth mover's distance to the future population for different predictors. A present population consists of all A/H3N2 HA sequences sampled in a 4 months time window. Quantities are averaged over all possible "present" populations from the year 2002. Predictors are: **Global consensus**: Consensus sequence of the present population. Best long-term predictor for a structure-less neutrally evolving population. **All present population**: All sequences in the present population. Perfect predictor if the population does not change at all through time. **Cluster-wise consensus**: Consensus sequence for each cluster in the present population. Clusters are based on local maxima of the LBI. Sequences are assigned to a given cluster based on their tree branch-length distance to the corresponding local maximum.

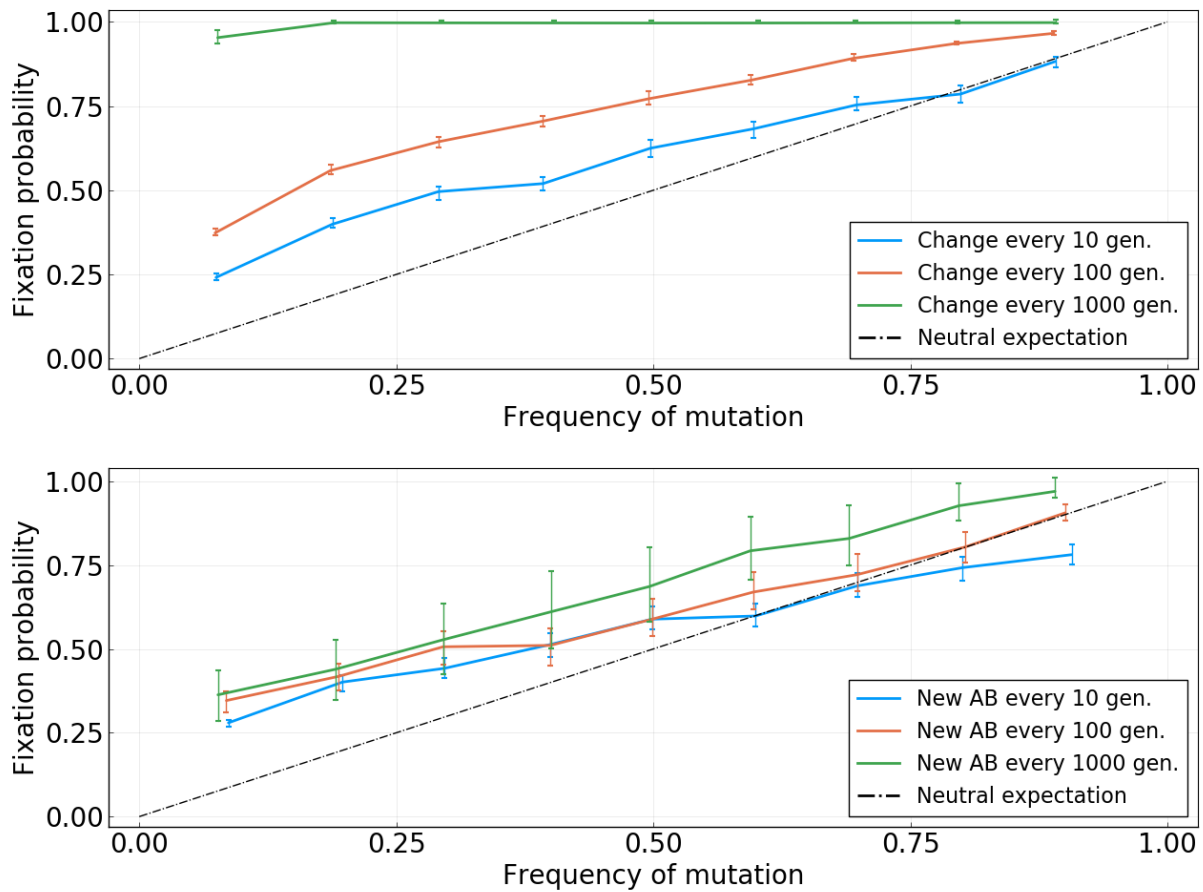


Figure S 16. Fixation probability as a function of frequency for the simulations discussed in the main text. **Top:** Simulation without antibodies. The three colored curves reflect different rate of change for the fitness landscape. Visual inspection of the frequency trajectories indicates a typical sweep time of ~ 400 generations. **Bottom:** Simulation with antibodies. The different colored curves indicate the rate at which antibodies are introduced.

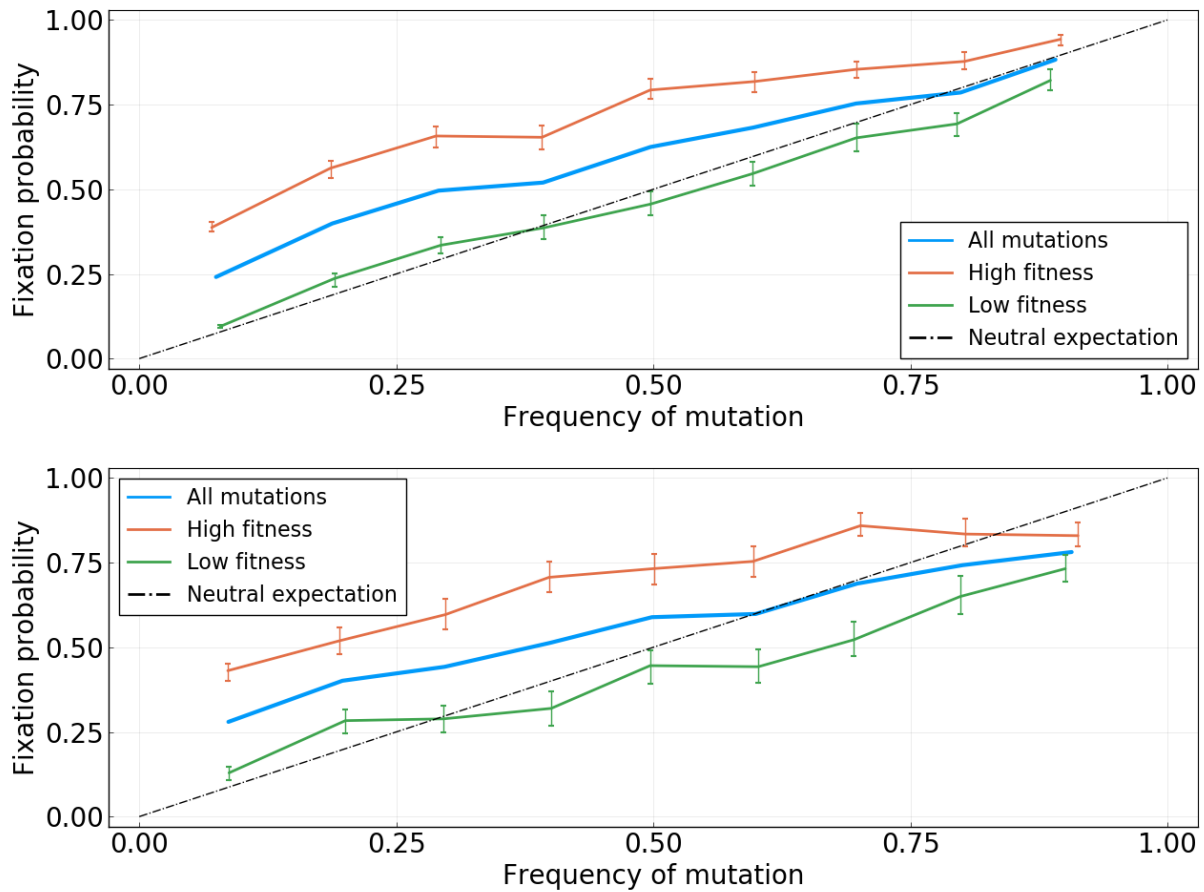


Figure S 17. Fixation probability as a function of frequency for the simulations discussed in the main text, with trajectories stratified according to real fitness values. “High” and “low” fitness classes are defined with respect to the median value. **Top:** Simulation without antibodies and with changes to the fitness landscape every $dt = 10$ generations. **Bottom:** Simulation with antibodies, with a new antibody every $dt = 10$ generations.